Article

Prediction of Streamflow Drought Index for Short-Term Hydrological Drought in the Semi-Arid Yesilirmak Basin Using Wavelet Transform and Artificial Intelligence Techniques

Okan Mert Katipoğlu *

Department of Civil Engineering, Erzincan Binali Yıldırım University, Erzincan 24002, Turkey

Abstract: The prediction of hydrological droughts is vital for surface and ground waters, reservoir levels, hydroelectric power generation, agricultural production, forest fires, climate change, and the survival of living things. This study aimed to forecast 1-month lead-time hydrological droughts in the Yesilirmak basin. For this purpose, support vector regression, Gaussian process regression, regression tree, and ensemble tree models were used alone and in combination with a discrete wavelet transform. Streamflow drought index values were used to determine hydrological droughts. The data were divided into 70% training (1969–1998) and 30% (1999–2011) testing. The performance of the models was evaluated according to various statistical criteria such as mean square error, root means square error, mean absolute error, and determination coefficient. As a result, it was determined that the prediction performance of the models obtained by decomposing into subcomponents with the discrete wavelet transform was optimal. In addition, the most effective drought-predicting model was obtained using the db10 wavelet and MGPR algorithm with mean squared error 0.007, root mean squared error 0.08, mean absolute error 0.04, and coefficient of determination (R^2) 0.99 at station 1413. The weakest model was the stand-alone FGSV (RMSE 0.88, RMSE 0.94, MAE 0.76, R^2 0.14). Moreover, it was revealed that the db10 main wavelet was more accurate in predicting short-term drought than other wavelets. These results provide essential information to decision-makers and planners to manage hydrological droughts in the Yesilirmak basin.

Keywords: hydrological drought; gaussian processes regression; machine learning; streamflow drought index; support vector regression; wavelet transform

1. Introduction

Drought is among the most dangerous natural disasters caused by a prolonged lack of water [1]. Droughts are classified as meteorological, agricultural, hydrological, and socioeconomic. Drought indicators have been developed for various regions and periods for each class. Meteorological and hydrological variables such as precipitation, current, temperature, potential evapotranspiration, solar radiation, crop data, and snowpack are used to calculate drought indices [2–4]. Predicting possible hydrological droughts in the future is of vital importance in terms of optimal operation of irrigation systems, agricultural production, the economy of the country, allocation of water for reservoir storage, determination of climate change effects, drought early warning, and management and planning of water resources [5]. In this respect, it is critical to develop effective drought forecasts to reduce the harmful effects of drought on nature and the environment. The Palmer hydrological drought index (PHDI), surface water supply index (SWSI), standardized runoff index (SRI), and streamflow drought index (SDI) are used to monitor hydrological droughts. Hydrological drought is defined as an extended period during which streamflow is below the predetermined threshold value of the Qg flow (the threshold level method was introduced by Yevjevich [6] in 1967). In order to determine episodes of hydrological drought, one of three methods is usually used: POT (peak over threshold), MA (moving average) and SPA (sequent peak algorithm) [7,8].

In the present study, the SDI was used to determine hydrological droughts because flows are the main component in monitoring the amount of surface water, and the index is easy to calculate [9].

Lack of precipitation and increased temperature significantly trigger hydrological droughts, reducing surface and underground runoff [10]. Hydrological drought is mainly due to decreases in various hydrological variables such as streamflow, lake and reservoir levels, and groundwater level [11]. SDI values, which are simple to calculate, are widely used to determine hydrological droughts [12–14]. The SDI is of great importance in terms of the decrease in water resources, deterioration in water quality, damage to coastal habitats, and reduction in agricultural production and hydroelectric power [15,16]. Accurate forecasting of droughts is important in preventing loss of life and property by reducing the risks and effects of drought, enabling the management of droughts through preparation and ensuring the health and well-being of those affected by transferring water to at-risk areas.

In recent years, the prediction of meteorological and hydrological droughts through artificial intelligence (AI) methods has become popular. There are many studies in the literature on drought prediction with AI [2,4,17–23]. Some examples of other prominent studies are given here: Borji, Malekian, Salajegheh, and Ghadimi [16] used support vector regression (SVR) and artificial neural networks (ANNs) to forecast hydrological drought in the Latian watershed in Iran. The long-term drought SVR algorithm predicted it more effectively than the ANN. Malik et al. [24] employed the coactive neuro-fuzzy inference system (CANFIS), the multi-layer perceptron neural network (MLPNN), and multiple linear regression (MLR) to predict hydrological drought in Uttarakhand State, India. According to various statistical criteria, the performance of the CANFIS models was best for hydrological drought prediction on the 1- to 3-, 6-, and 12-month timescales, while the MLPNN was best on the 1- to 6- and 9-month timescales. Moreover, the MLR model was the best on the 24-month time scale. Wavelet decomposition (WD) is a mathematical transformation function used to obtain signals' time-frequency representation [25]. Özger et al. [26] employed an ANN and support vector machine (SVM) with empirical mode decomposition (EMD) and WD for 1-, 3-, and 6-month lead-time prediction of the self-calibrated Palmer drought severity index in the Adana and Antalya provinces in Turkey. Predictions made with the WD combination were superior to those made with EMD. Malik and Kumar [27] used MLPNN, CANFIS, and MLR to forecast meteorological drought in Uttarakhand State, India. According to the Taylor diagram and various statistical criteria, the CANFIS and MLPNN models are superior to MLR for forecasting meteorological drought. Ahmadi, Mehdizadeh, and Mohammadi [28] applied single SVR and hybrid SVR with two bio-inspired- and wavelet-based techniques to predict Iran's reconnaissance drought index (RDI). The wavelet–SVR (W–SVR) model, divided into subcomponents with the db4(2) wavelet at the Tehran station, achieved the most effective results in RDI estimation. Aghelpour, Bahrami-Pichaghchi, and Varshavian [5] employed the stochastic-based autoregressive moving average (ARMA), the machine learning-based adaptive neuro-fuzzy inference system (ANFIS), and the group method of data handling (GMDH) to predict hydrological drought with SDI in northern Iran. As a result, it was determined that stochastic models can be used for hydrological drought prediction. Karbasi et al. [29] used Gaussian process regression (GPR), cascade-NN, and MLPNN alone and in combination with a wavelet transform (WT) to predict meteorological drought in Iran 1 and 6 months ahead. According to the results of that study, wavelet-based models will increase the accuracy of drought prediction; in particular, the Meyer wavelet and W–GPR and W–cascade-NN models are superior. Mohamadi et al. [20] used the nomadic people optimization algorithm (NPA) and various machine learning algorithms to model the spatial–temporal pattern of droughts in Iran. It was determined that the ANFIS–NPA and MLP–NPA models performed better than other hybrid models. Achite et al. [30] used the Bayesian averaging model with multiple hybrid artificial neural network models to model the standardized precipitation index. As a result of the study, it was determined that the ANN-salp swarm algorithm, ANN-sine cosine algorithm, ANN-particle swarm

optimization, and ANN-water strider technique improved ANN model success. Elbelt-agi et al. [31] estimated standardized precipitation index (SPI) values In Jaisalmer, India, by combining the random subspace (RSS), M5 pruning tree (M5P), random forest (RF), and random tree (RT) models. It has been revealed that M5P algorithms increase the success of RSS. Kumar et al. [32] used the Indian Meteorological Department (IMD) criteria and the standardized precipitation index to evaluate meteorological droughts in the Indian State of Uttarakhand. As a result of the study, it has been determined that droughts can be analyzed more successfully. When the existing literature is examined, it is noted that the prediction of hydrological droughts with wavelet-based hybrid machine learning models takes up little space. For this reason, hydrological drought was predicted by combining various WTs and machine learning methods in the present study.

WTs are mathematical functions used to reduce and compress noise in time series. In the present study, we aimed to improve model performance by using a WT together with various artificial intelligence techniques. The WT splits a signal into a shifted and scaled version of the original (or mother) wavelet. Another aim of the present study was to determine the most effective machine learning model and mother wavelet in predicting hydrological droughts with a 1-month lead time. We also investigated which mother wavelet and machine learning techniques gave the most accurate results in predicting short-term drought. Monthly SDI values were calculated, and hydrological droughts were estimated using various delayed SDI values as inputs. SVR, GPR, RT, ensemble tree, and eXtreme gradient boosting (XGBOOST) models in the MATLAB software regression learner toolbox and the software R version 4.2.2 were used to set up the models. The performance and current status of tree-based, kernel-based, and reinforced tree-based models in drought prediction were evaluated. In addition, hybrid wavelet–machine learning models were used to improve models' prediction success. The input values were divided into sub-signals with Db10, Haar, Sym8, and Coif5 wavelets, which are widely used in hydrological and meteorological studies. The study provides innovation in comprehensively comparing and integrating the success of Db10, Haar, Sym8, and Coif5 mother wavelets and various machine learning models in predicting future hydrological droughts. The study outputs have contributed to a better understanding of how hydrological drought conditions can be modeled and monitored and how they can be managed and mitigated. This information is vital for developing drought preparedness and response strategies and informing water resource management policies and practices. In addition, accurate estimation of hydrological droughts contributes to revealing the complex interactions between the water cycle, climate, and land use.

2. Materials and Method

2.1. Study Area and Data

The area of Yeşilırmak basin is approximately 39,600 km^2. The annual average precipitation of the basin, which is under the effects of the Black Sea climate, is 528 mm/m^2, the average yearly flow is 6.10 km^3, and the average annual temperature is 12 °C. In the Yesilirmak basin, the climate is typically dry and hot during the summer months, with temperatures often reaching into the high 30s Celsius. The winter months are generally cooler, ranging from freezing to the low teens Celsius [33,34]. Morphological conditions refer to the physical characteristics of the area that make up the shape and characteristics of the land. The Yeşilırmak basin is located in a rugged region with a variable landscape, including rolling hills, valleys, and mountains. The region's altitude ranges from about 100 meters above sea level to 2000 meters above sea level. The basin also has a variety of vegetation, including forests, grasslands, and farmland [35]. Yesilirmak river is one of the longest rivers in Turkey. The flow of these rivers can vary significantly depending on the time of year and the amount of precipitation in the area. During the rainy months, the rivers in the Yeşilırmak basin may have higher flow levels, while during the dry months, the flow may decrease. There are many lakes in the Yeşilırmak basin, especially Samsun Lake and Eymir Lake. These lakes are used for irrigation, drinking water, and recreational activities.

In addition, since the number of dam lakes in the basin is higher than in other basins in Turkey, it is of critical importance for areas such as hydroelectricity generation, irrigation, and drinking and industrial water. As a consequence, assessment of the hydrological drought situation of the basin is critical [36].

The study shows boxplot diagrams of the selected streamflow observation stations in the Yesilirmak basin (Figure 1). The mean monthly streamflow data of the stations used—1401, 1413, and 1414—were obtained from the streamflow yearbooks of the general directorate of electric power resources survey and development administration. Average monthly streamflow data from 1969 to 2011 were used to calculate SDI values. According to Katipoglu, Yeşilyurt, and Dalkılıç [37], examination revealed that the monthly and annual SDI trends with the Mann-Kendall test in 7 flow stations in the Yeşilırmak basin. In their study, while there was no statistically significant trend in annual SDI values at station 1401, significant decreasing trends were detected at stations 1413 and 1414. These results show that station 1401 is stationary, while stations 1413 and 1414 are non-stationary. In Figure 2, change graphs compare the station-based changes of monthly and annual average streamflows. Accordingly, while the annual average streamflows at station 1401 show a constant change, the streamflows at stations 1413 and 1414 show a significant trend in terms of decreases and increases (Figure 2a). This situation supports the conclusion that while station 1401 is stationary, stations 1413 and 1414 are non-stationary. When the monthly variation of the streamflows is analyzed, it is seen that the streamflow values at station 1401 are the largest and the streamflow values at station 1414 are the lowest (Figure 2b). In Figure 2c, which evaluates the seasonal variation of the flows, it is noteworthy that while the streamflows at stations 1401 and 1413 increase in spring, they decrease in summer. At station 1414, on the other hand, no significant seasonal change was observed. The locations of the flow observation stations used in the Yesilirmak Basin are shown in Figure 3.
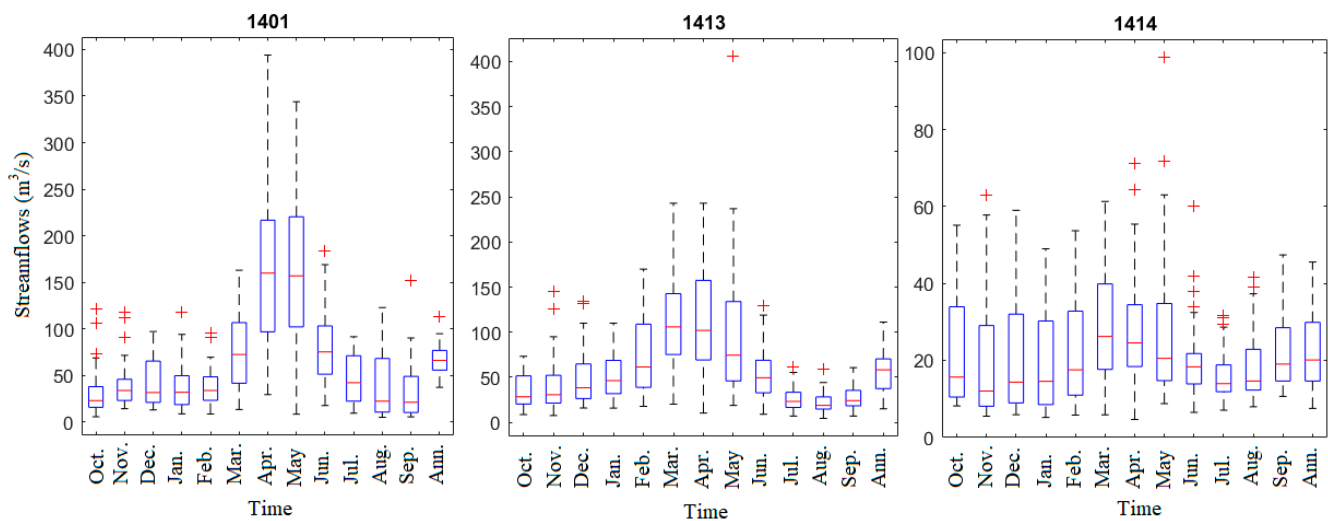

Figure 1. Boxplots of the mean monthly streamflows used in the study.

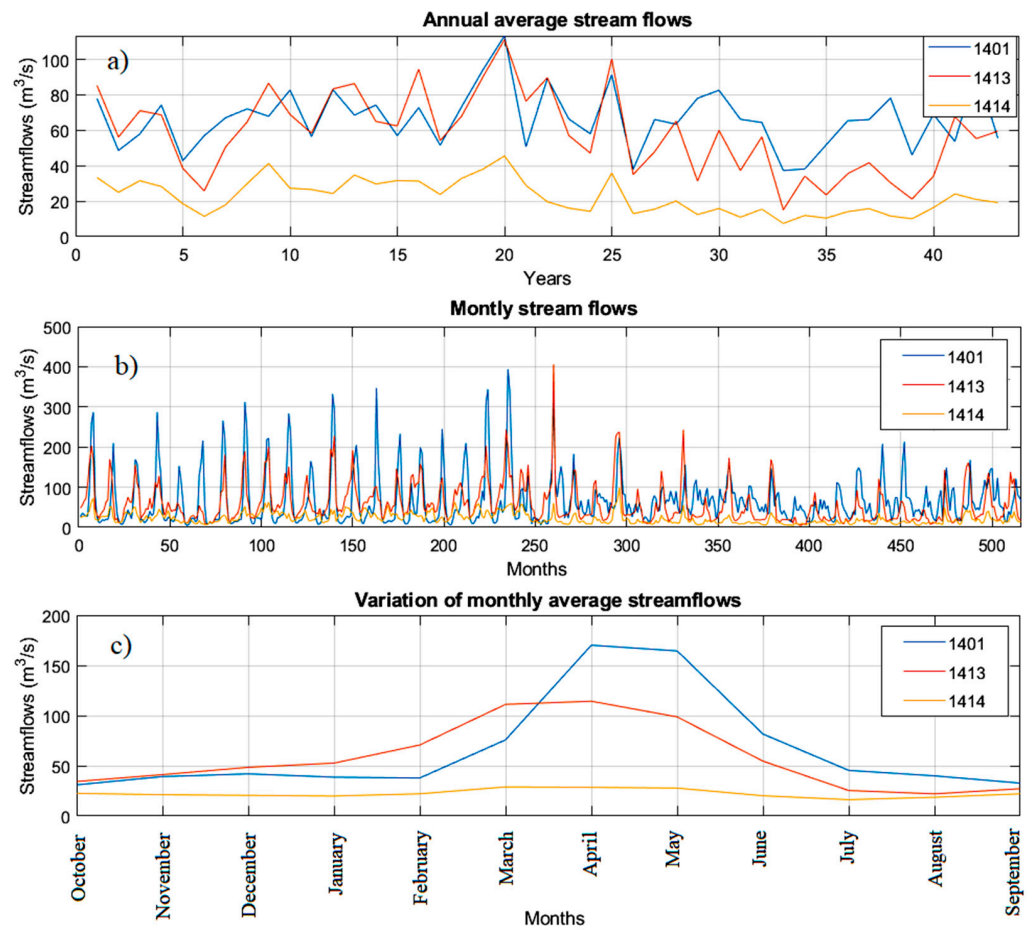**Figure 2.** Variation of monthly and annual streamflows: (**a**) variation of monthly average streamflows (**b**) variation of annual average streamflows (**c**) variation of the seasonal streamflows.
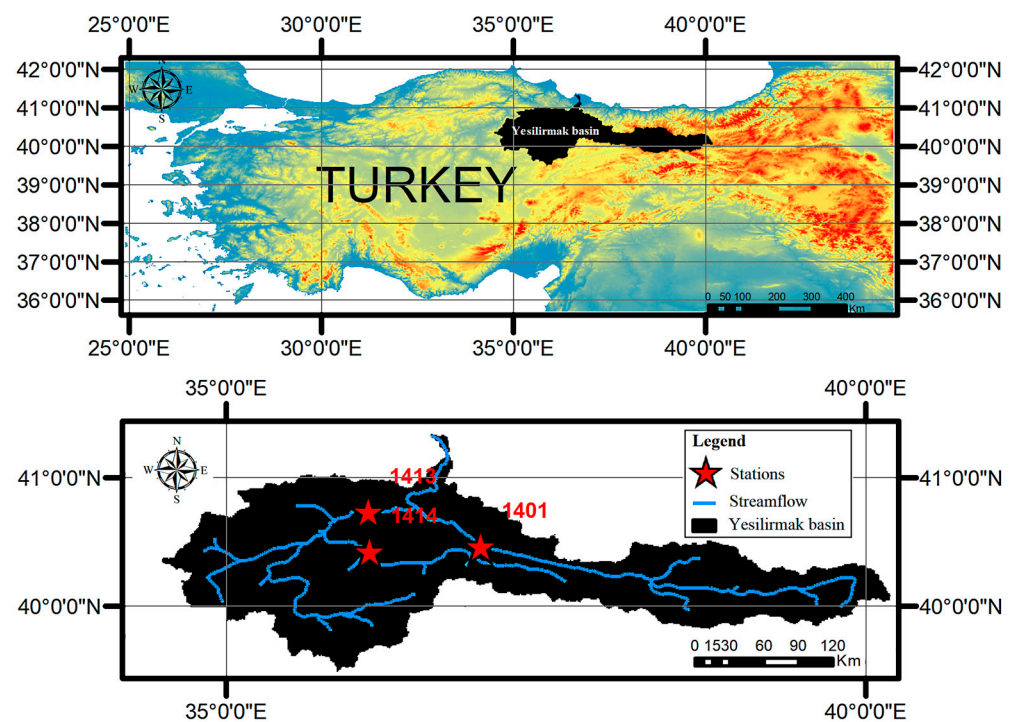

Figure 3. Yesilirmak Basin location map.

2.2. Streamflow Drought İndex (SDI)

The SDI was first proposed by Nalbantis [9] to evaluate hydrological drought characteristics such as duration, intensity, and intensity on multiple time scales. The calculation procedure for SDI values is similar to that for SPI [38], i.e., streamflow values replace precipitation values. The SDI values are calculated via Equation (1):

$$\text{SDI}_{i,k} = \frac{V_{i,k} - \bar{V}_k}{S_k} \quad i = 1, 2, \ldots k = 1, 2, 3, 4, \ldots, \tag{1}$$

where $V_{i,k}$ is streamflow volume for the *k*th month in the *i*th hydrological year and $\bar{V}_k$ and S_k are the mean and the standard deviation of streamflow volumes in the *k*th month over the study period. Within the scope of the study, calculations were made with the drought indices calculator software (DrinC), which provides an interface for the calculation of meteorological, hydrological, and agricultural drought indices. Drought classes and probabilities in the basin according to SDI values are presented in Table 1.

Table 1. Drought classification by SDI value and corresponding probabilities [23].

SDI Value	Category	Probability (%)
SDI >= 2.00	Extremely wet	1.94
1.50 <= SDI < 2.00	Severely wet	3.29
1.00 <= SDI < 1.50	Moderately wet	10.85
0.00 <= SDI < 1.00	Mildly wet	32.17
−1.00 <= SDI < 0.00	Mild drought	32.95
−1.50 <= SDI < −1.00	Moderate drought	14.15
−2.00 <= SDI < −1.50	Severe drought	3.49
SDI <= −2.00	Extreme drought	1.16

The main factors affecting the SDI values are precipitation, runoff, evapotranspiration, temperature, soil moisture and land use. In addition, SDI is affected by a combination of these factors, and the relative importance of each element may vary depending on the particular location and climatic conditions [39,40]. The main advantages of SDI values are that they are easy to measure and observe and have flexible temporal and spatial scales. In addition, it is directly connected to the streamflow, which is a physical feature [13,14].

2.3. Selection of Input Parameters

Selecting the best input and output variables significantly influences modeling success, especially nonlinear hydrological processes.

$$\text{ACF}_k = \frac{\sum_{t=1}^{N-k}(Y_t - \bar{Y})(Y_{t+k} - \bar{Y})}{\sum_{t=1}^{N}(Y_t - \bar{Y})} \tag{2}$$

where *N* is the number of observations, *k* is the delay value in the Y_t series, and $\bar{Y}$ indicates the average of the series. For *k*th delays, the ACF and PACF are stated as in Equations (2) and (3) [27,41,42].

$$PACF_{k,k} = \frac{ACF - \sum_{j=1}^{k-1} PACF_{k-1,j}ACF_{k-1}}{1 - \sum_{j=1}^{k-1} PACF_{k-1,j}ACF_{k-1}} \tag{3}$$

PACF values calculated for *k*th delays were evaluated according to upper and lower critical limits at 5% significance level calculated by Equation (4):

$$\text{CL}_{\text{upper/lower}} = \pm \frac{1.96}{\sqrt{N}} \tag{4}$$

2.4. Machine Learning Models

In this study SVR, GPR, RT, ET, and XGBOOST models were used. The various kernel and tree types of these models are detailed as follows: fine tree (FT), medium tree (MT), coarse tree (CT), linear SVR (LSVR), quadratic SVR (QSVR), cubic SVR (CSVR), fine Gaussian SVR (FGSVR), medium Gaussian SVR (MGSVR), coarse Gaussian SVR (CGSVR), boosted tree (BT), bagged tree (BAT), squared exponential GPR (SEGPR), Matern 5/2 GPR (MGPR), exponential GPR (EGPR), and rational quadratic GPR (RQGPR) models were used to predict hydrological droughts.

2.4.1. Support Vector Machine (SVM)

SVM, a supervised learning method developed by Vapnik [43], is based on the statistical theory of learning (Vapnik–Chervonenkis theory) and generates a good generalization capacity [44]. SVMs provide a unique solution for a given dataset, unlike other algorithms that may have multiple solutions or local optima. They are also relatively robust against overfitting, especially when using the "kernel trick" that projects data into a higher dimensional space to find a nonlinear decision boundary. SVR refers to the use of SVM for regression purposes [45]. The SVR is calculated by Equation (5) by mapping between input and output. The SVR function reveals the relationship between predictor and response [43]:

$$f(x) = (w, \Phi(x)) + b, \tag{5}$$

where $f(x)$ is a high dimensional feature space, w is a weight of the output variable, and b is the bias term. In the present study, various kernel functions' performances were compared to select the most suitable SVM model. The kernel function indicates the type of transformation applied to the SVM model [46,47]. QSVR, CSVR, FGSVR, MGSVR, and CGSVR models were used.

2.4.2. Gaussian Processes Regression (GPR)

GPR is a flexible non-parametric data modeling method. It is a member of the family of stochastic processes [48]. It is a non-parametric kernel-based probability technique with the infinite-dimensional generalization of multivariate normal distributions. These models are also used in statistical modeling, regression analysis, and mapping analysis [49]. There are four different models with different kernels: exponential, Matern 5/2, squared exponential, and rational quadratic [50]. The kernel function is the most important part of GPR. The kernel function shows the similarity between the data in supervised learning [51,52]. The equations of the kernel functions used are given below:

Squared Exponential Kernel:

$$k(x_i, x_j \mid \theta) = \sigma_f^2 \exp\left[-\frac{1}{2} \frac{(x_i - x_j)^T (x_i - x_j)}{\sigma_l^2} \right]$$

Exponential Kernel:

$$k(x_i, x_j \mid \theta) = \sigma_f^2 \exp\left[-\frac{r}{\sigma_l} \right]$$

Matern 3/2:

$$k(x_i, x_j \mid \theta) = \sigma_f^2 \left(1 + \frac{\sqrt{3}r}{\sigma_l} \right) \exp\left[-\frac{\sqrt{3}r}{\sigma_l} \right]$$

Matern 5/2:

$$k(x_i, x_j \mid \theta) = \sigma_f^2 \left(1 + \frac{\sqrt{5}r}{\sigma_l} + \frac{5r^2}{3\sigma_l^2} \right) \exp\left[-\frac{\sqrt{5}r}{\sigma_l} \right]$$

Rational Quadratic Kernel:

$$k(x_i, x_j \mid \theta) = \sigma_f^2 \left(1 + \frac{r^2}{2\alpha\sigma_l^2} \right)^{-\alpha}$$

where $r = \sqrt{(x_i - x_j)^T (x_i - x_j)}$ shows the Euclidean distance between x_i and x_j, σ_l indicates the characteristic length scale, and σ_f denotes the standard deviation of signal [51,52].

2.4.3. Regression Tree (RT)

An RT uses a tree structure to predict new data via training data. Unlike linear regression, which represents all data, RTs divide the area into smaller regions with the most homogeneous results. This method involves splitting a tree into smaller branches called nodes, and a single leaf at the end is expressed as an end node [38]. There are three types of RTs in the regression learner toolbox, i.e., FTs, MTs, and CTs. Future droughts were predicted by training these trees. A fine tree with many small leaves may perform well in the training phase but poorly in the testing phase. A very leafy tree tends to overfit, and validation accuracy is often much lower than training accuracy. Conversely, a coarse tree with fewer large leaves may have better test success and lower training success [14]. Depending on the depth of the tree and the number of leaves, RTs are expressed as FTs, CTs, and MTs. FTs have more leaves and higher prediction success. Moreover, this tree type is suitable for large class datasets. CTs have a minimal number of leaves but show minimal accuracy. MTs have a reasonable number of leaves [13].

2.4.4. Ensembles of Trees (ET)

Ensemble models are widely used for hydrological simulation and prediction purposes [53]. These models aggregate the results of many weak models into a single high-quality ensemble model. In the present study, drought estimation was performed with the commonly used BT and BAT algorithms. BT combines the outputs from a base model set to increase the final model's success [54,55]. BAT combines all trees to obtain a unified tree model. It also considers the average of all predictions from different trees to increase prediction success [56]. In the present study, ensemble trees were used in the MATLAB regression learner toolbox (Table 2).

Table 2. The types of ensembles of trees [57].

Regression Model Type	Interpretability	Ensemble Method
Boosted Trees	Hard	Least-squares boosting (LSBoost)
Bagged Trees	Hard	Bootstrap aggregating or bagging

2.4.5. eXtreme Gradient Boosting (XGBOOST)

XGBOOST is an algorithm based on gradient boosting. It trains different models sequentially to improve previously used models. Thus, it reduces the bias of the established model. The XGBOOST model is an effective algorithm for overfitting [58]. It determines the sum of leaf weights in a decision tree and calculates the outputs by summing all the weights in the decision tree. The XGBOOST algorithm selects the split threshold for each tree node and determines the most appropriate weights [59,60]. The general hyperparameters of model are selected by default as follows. The gblinear booster, max.depth = 3, eta = 1, nthread = 2, nrounds = 500.

2.5. Wavelet Transformation (WT)

In recent years, wavelet transform has played an important role in hydrology and climatology. WT is a time series analysis suggested to overcome Fourier series shortcomings [61]. It is a multiple decomposition technique that provides important information regarding the signal's time and frequency domains. It can also evaluate the original time series in both time and frequency domains by decomposing them in different frequency bands using wavelet functions. The primary purpose of decomposing the original series into various decomposition levels is to reveal helpful information [4,28]. A wavelet transform consists of three essential components: scale, the transmission coefficient, and the main wavelet. The mother wavelet is shown in Equation (6):

$$\int_{-\infty}^{+\infty} \Psi(t) dt = 0 \tag{6}$$

The wavelet performs the time series decomposition with Equation (7):

$$\Psi = 2^{\frac{-j}{2}} \int_{1}^{j} \Psi\left(2^{\frac{-j}{2}} - k\right) f(t) dt \tag{7}$$

where Ψ shows the discrete wavelet transform, $f(t)$ represents the time series, j is the decomposition level, and k is the origin length [28,62].

When applying the WT, it is necessary to specify the optimal number of decomposition levels according to the dataset. The number of decomposition levels is calculated by Equation (8). This value depends on signal length [63,64].

$$L = int[log(N)], \tag{8}$$

where L is the decomposition level and N is the number of samples. In the present study, hybrid wavelet–machine learning models were established using discrete WT and machine learning models. Db10, Haar, Sym8, and Coif5 mother wavelets were used to subdivide the input variables.

2.6. Performance Evaluation

The prediction accuracy of the developed SVR, GPR, DT, ET and XGBOOST models was made by testing various statistical criteria. These are values of mean square error (MSE), root means square error (RMSE), mean absolute error (MAE), and determination coefficient (R^2). The MSE and RMSE values closer to 0 and the R^2 values closer to 1 indicate that the estimation accuracy has increased [52]. The statistical calculations can be obtained by Equations (9), (10), (11), and (12), respectively, where $SDI_{a,i}$ denotes actual values, $SDI_{p,i}$ denotes the predicted values of models, $SDI_{a,i}$–$SDI_{p,i}$ denotes the value of the error terms, $SDI_{a,avg}$ denotes average of SDI values, and n denotes the number of data. The model with a higher R^2 value and lower MSE, RMSE, and MAE value was determined to be more successful in drought prediction. Table 3 shows the equation, optimal values and ranges of performance criteria used to evaluate the success of artificial intelligence models.

Table 3. Model performance evaluation criteria [65,66].

Performance Evaluation Criteria		Range	Best Values
$MSE = \frac{1}{n}\sum_{i=1}^{n}\left(SDI_{a,i} - SDI_{p,i}\right)^2$	(9)	0 to ∞	0
$MAE = \frac{1}{n}\sum_{i=1}^{n}\left\|SDI_{a,i} - SDI_{p,i}\right\|$	(10)	0 to ∞	0
$RMSE = \sqrt{\frac{1}{n}\sum_{i=1}^{n}\left(SDI_{a,i} - SDI_{p,i}\right)^2}$	(11)	0 to ∞	0
$R^2 = \frac{\sum_{i=1}^{n}\left(SDI_{a,i} - SDI_{a,avg}\right)^2 - \sum_{i=1}^{n}\left(SDI_{a,i} - SDI_{p,i}\right)^2}{\sum_{i=1}^{n}\left(SDI_{a,i} - SDI_{a,avg}\right)^2}$	(12)	−1 to +1	1

3. Methodology

In this study, Stand-alone SVR, GPR, DT, ET and XGBOOST models were established for the estimation of SDI values and the inputs were separated into sub-signals with discrete wavelet transform to improve the model performance. Db10, Haar, Sym8, and Coif5 mother wavelets, which are the most widely used in hydrology, are used to subdivide SDI time series. Hybrid and stand-alone algorithms that show the most accurate prediction results according to various performance criteria have been determined. The flow chart showing the application steps of the study is presented in Figure 4.
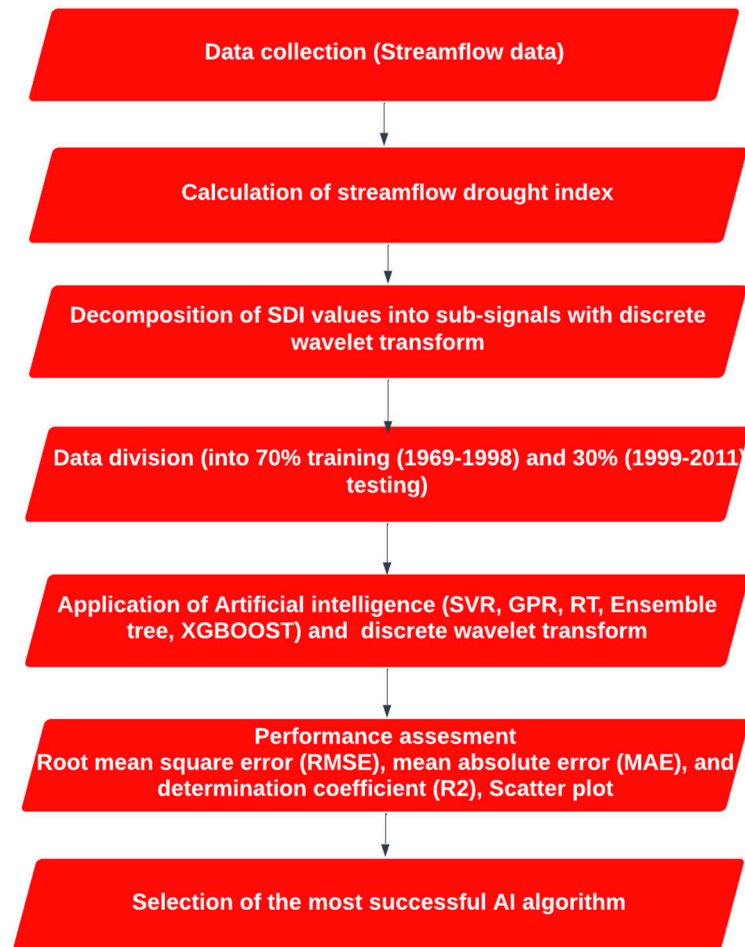
Figure 4. Flow chart of the study.

4. Results

4.1. Input Selection and Establishment of Machine Learning Models

This study aims to predict the SDI values of the following month by applying the SVR, GPR, RT, and ET models. For this purpose, the SDI time series is divided into 70% training and 30% testing. For the selection of input parameters, output values SDI(t + 1) autocorrelation and partial autocorrelation functions (ACF and PACF) were examined. According to the graphs of these functions, the values exceeding the 95% confidence limit of the lagged SDI values were presented as input to the model. Lagged values of ACF and PACF calculated by Equations (2) and (3) are shown in Figure 5. The lagged values of the outputs exceeding the 95% confidence limits calculated through Equation (4) were chosen as the model's input [27,41,42]. When the ACF and PACF graphs are considered together, it was seen that the stations with a delay of 1, 2, 8, 9, 11, and 12 months at station 1401, and stations with a delay of 1, 2, 3, 4, 9 and 11 months at station 1413 exceed 95% confidence limits. In addition, it was revealed that the streamflow values with 1, 2, 8-, 9-, 10- and

12-months delay in station 1414 have an autocorrelation. Therefore, artificial intelligence model combinations were established according to this approach.
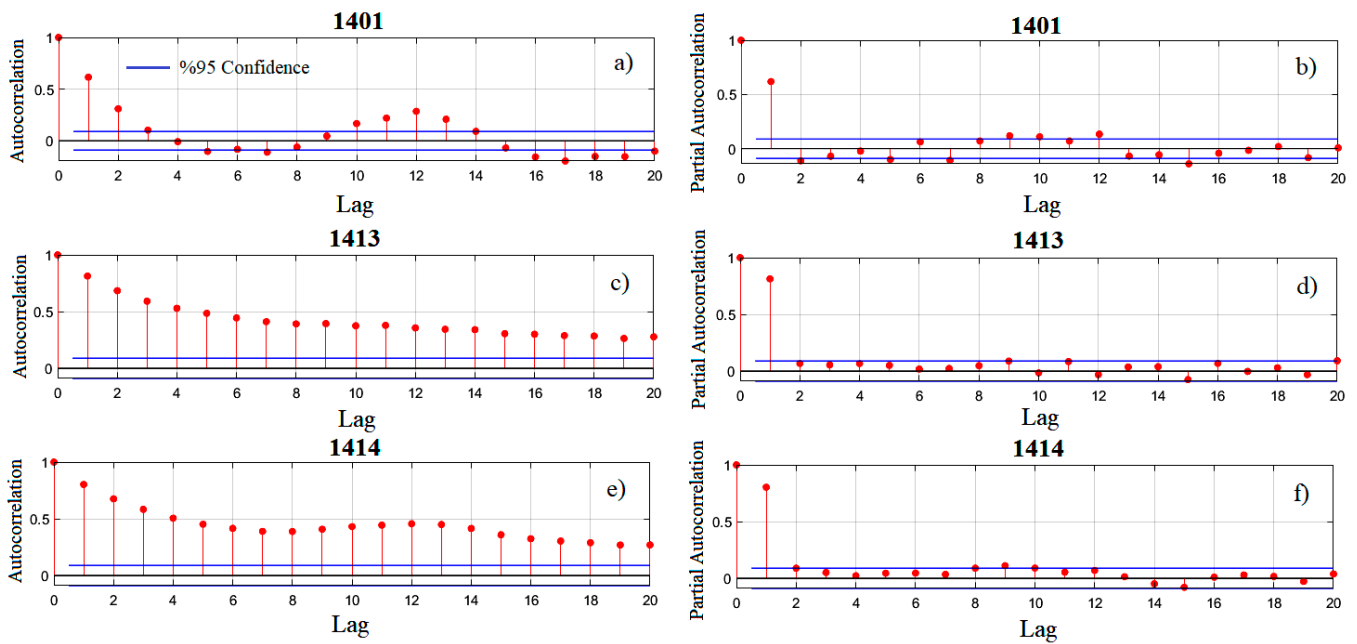
Figure 5. The correlograms of the SDI values: (**a**) ACF of station 1401; (**b**) PACF of station 1401; (**c**) ACF of station 1413; (**d**) PACF of station 1413; (**e**) ACF of station 1414; (**f**) PACF of station 1414.

According to the ACF and PACF graphs, the 1, 2, 8, 9, 10, 12-month lagged components of the SDI(t + 1) values at station 1401 were presented as inputs to the machine learning models since they exceeded the 95% confidence limit. At stations 1413 and 1414, 1, 2, 3, 4, 9, 11 and 1, 2, 8, 9, 10, 12 months lagged components of SDI(t + 1) values, respectively, were selected as inputs to the models (Figure 5 and Table 4).

Table 4. Established model structures.

	Input	Output
1401	SDI(t-11), SDI(t-9), SDI(t-8), SDI(t-7), SDI(t-1), SDI(t)	SDI(t + 1)
1413	SDI(t-10), SDI(t-8), SDI(t-3), SDI(t-2), SDI(t-1), SDI(t)	SDI(t + 1)
1414	SDI(t-11), SDI(t-9), SDI(t-8), SDI(t-7), SDI(t-1), SDI(t)	SDI(t + 1)

In the present study, the decomposition level was chosen as two according to the $L = \text{Int}[\log 498] = 2$. Then, the obtained sub-signals were subjected to correlation analysis with the output of W–ML models (SDI(t + 1)) and the most suitable input combinations were determined. In Figure 6, we present the sub-series of input values with high autocorrelation at station 1401, selected as an example, produced by the db 10 mother wavelet.

Table 5 shows the correlation coefficients of the delayed SDI values separated into sub-signals by the discrete wavelet transform. According to [67], values above 0.2 were used in hybrid W–ML models. Therefore, when Table 5 is examined, it is generally presented as an input to the W–ML models, as the approximate components have high correlations. In addition, the polar diagram showing the correlation coefficients of the subcomponents is demonstrated in Figure 7.
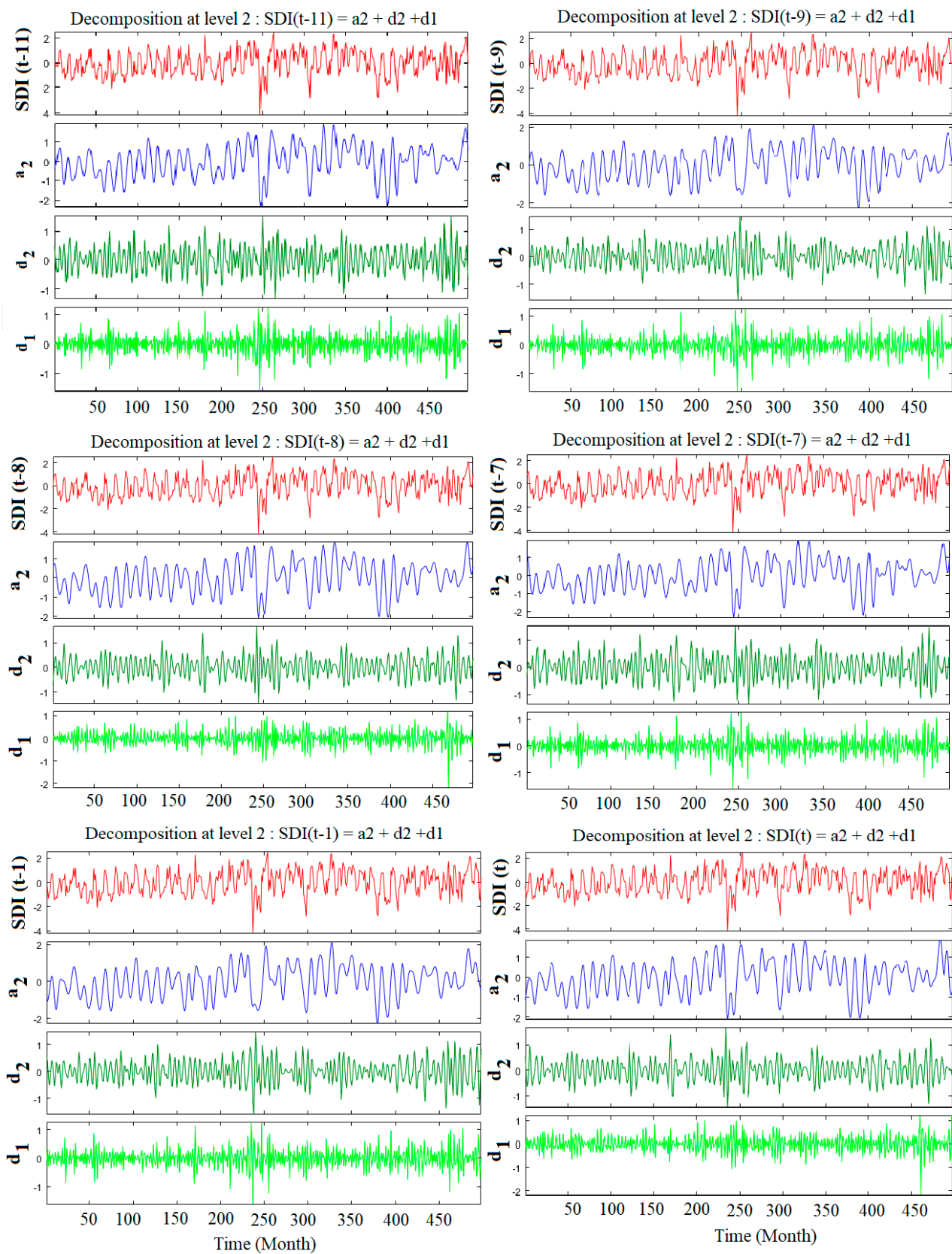
Figure 6. Subcomponents of selected input values of station 1401 were obtained by discrete wavelet transform.

Table 5. The relationship of the subcomponents separated by various mother wavelets with SDI (t + 1).

		1401			
		db 10	**Haar**	**Sym 8**	**Coif 5**
SDI (t-11)	d1	0.06	0.02	0.02	0.02
	d2	0.09	−0.04	0.09	0.07
	a2	**0.29**	**0.36**	**0.30**	**0.31**
SDI (t-9)	d1	0.02	0.05	0.04	0.04
	d2	−0.04	0.10	0.01	−0.02
	a2	**0.22**	0.14	0.19	**0.21**
SDI (t-8)	d1	0.01	−0.01	0.00	0.00
	d2	−0.10	0.09	−0.03	−0.05
	a2	0.11	0.02	0.07	0.08
SDI (t-7)	d1	−0.02	0.02	−0.01	−0.01
	d2	−0.05	0.01	−0.05	−0.04
	a2	−0.05	−0.09	−0.05	−0.06
SDI (t-1)	d1	−0.05	−0.04	−0.08	−0.08
	d2	−0.28	−0.12	−0.29	−0.26
	a2	**0.55**	**0.58**	**0.58**	**0.57**
SDI (t)	d1	−0.22	−0.03	−0.14	−0.16
	d2	**0.24**	0.11	0.10	0.11
	a2	**0.73**	**0.77**	**0.75**	**0.76**
		1413			
SDI (t-10)	d1	0.03	0.03	0.03	0.03
	d2	−0.03	0.01	−0.04	−0.04
	a2	**0.42**	**0.41**	**0.42**	**0.42**
SDI (t-8)	d1	0.03	0.01	0.02	0.02
	d2	−0.03	−0.02	−0.01	−0.03
	a2	**0.43**	**0.45**	**0.43**	**0.43**
SDI (t-3)	d1	0.02	−0.01	0.00	0.00
	d2	−0.07	−0.03	−0.05	−0.04
	a2	**0.60**	**0.60**	**0.60**	**0.59**
SDI (t-2)	d1	0.06	−0.02	0.05	0.05
	d2	−0.22	−0.08	−0.22	−0.22
	a2	**0.72**	**0.69**	**0.71**	**0.71**
SDI (t-1)	d1	−0.05	−0.01	−0.02	−0.02
	d2	−0.18	−0.02	−0.18	−0.18
	a2	**0.82**	**0.79**	**0.82**	**0.82**
SDI (t)	d1	−0.15	−0.06	−0.13	−0.13
	d2	0.11	0.18	0.11	0.10
	a2	**0.89**	**0.87**	**0.89**	**0.89**
		1414			
SDI (t-9)	d1	0.02	0.01	0.00	0.00
	d2	−0.06	0.03	−0.02	−0.03
	a2	**0.49**	**0.48**	**0.49**	**0.49**
SDI (t-8)	d1	0.00	0.01	0.00	0.00
	d2	−0.03	−0.02	−0.02	−0.03
	a2	**0.46**	**0.47**	**0.46**	**0.46**
SDI (t-7)	d1	−0.02	−0.01	0.01	0.01
	d2	0.02	−0.04	−0.01	−0.02
	a2	**0.43**	**0.45**	**0.43**	**0.43**
SDI (t-1)	d1	−0.04	−0.01	−0.03	−0.03
	d2	−0.18	−0.04	−0.18	−0.18
	a2	**0.81**	**0.79**	**0.81**	**0.81**
SDI (t)	d1	−0.16	−0.07	−0.13	−0.14
	d2	0.13	0.16	0.10	0.09
	a2	**0.88**	**0.87**	**0.89**	**0.89**

Note: Bold characters indicate lagged SDI values selected as inputs to W–ML models.
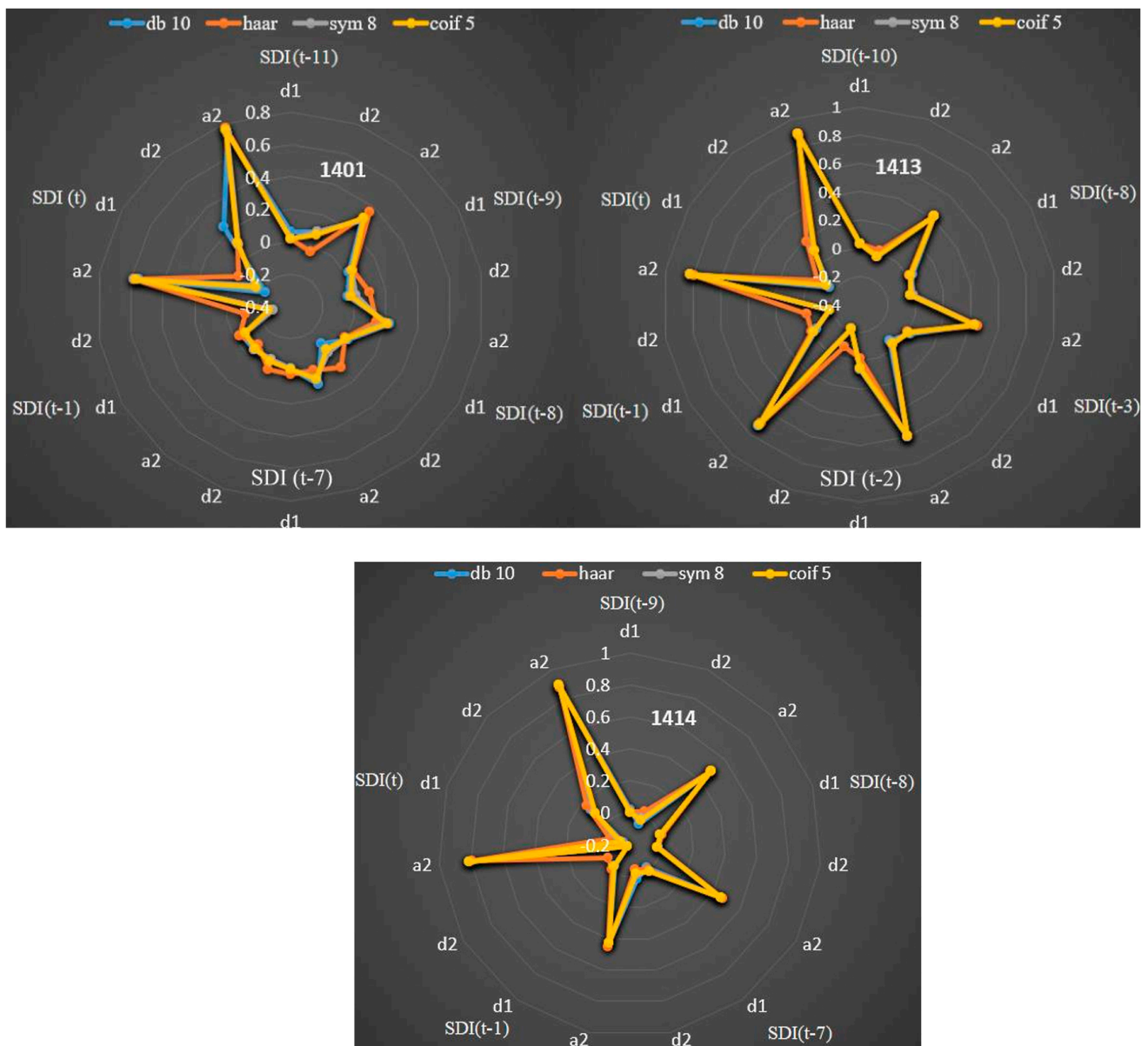
Figure 7. Correlation polar plot of wavelet subcomponents.

4.2. Comparison of Machine Learning Models

In this study, the performances of various machine learning models such as FT, MT, CT, LSVR, QSVR, CSVR, FGSVR, MGSVR, CGSVR, BT, BAT, SEGPR, MGPR, EGPR, and RQGPR in predicting hydrological droughts were evaluated. In Table 6, the drought prediction results at station 1401 are presented. Statistical criteria such as MSE, RMSE, MAE, and R^2 were tested to select the optimal model. The smallest error values and the highest coefficients of the determination indicate the optimal model. According to these criteria, the most successful stand-alone machine learning (ML) model at station 1401 is XGBOOST. In addition, the XGBOOST model used with the db10 wavelet showed the most accurate results for predicting SDI values.

Table 6. Drought prediction results at the streamflow observation station 1401.

Statistic	Method	FT	MT	CT	LSVR	QSVR	CSVR	FGSVR**	MGSVR	CGSVR	BT	BAT	SEGPR	MGPR	EGPR	RQGPR	XGBOOST*
					Mother wavelet type: No (Stand-alone ML)												
Train	MSE	0.87	0.69	0.67	0.59	0.65	0.83	0.88	0.62	0.60	0.64	0.62	0.62	0.60	0.59	0.60	**0.61**
	RMSE	0.94	0.83	0.82	0.77	0.81	0.91	0.94	0.77	0.78	0.80	0.80	0.79	0.77	0.77	0.77	**0.78**
	MAE	0.72	0.64	0.63	0.58	0.60	0.64	0.76	0.59	0.59	0.60	0.60	0.59	0.58	0.58	0.58	**0.60**
	R^2	0.15	0.33	0.35	0.42	0.37	0.19	0.14	0.40	0.42	0.38	0.38	0.40	0.42	0.43	0.42	**0.40**
Test	MSE	0.99	0.79	0.77	0.66	0.75	0.82	0.88	0.76	0.65	0.71	0.69	0.69	0.69	0.68	0.69	**0.58**
	RMSE	0.99	0.89	0.87	0.82	0.86	0.90	0.94	0.87	0.81	0.84	0.83	0.83	0.83	0.82	0.83	**0.76**
	MAE	0.78	0.68	0.68	0.64	0.68	0.71	0.76	0.70	0.64	0.66	0.64	0.66	0.65	0.65	0.65	**0.63**
	R^2	0.22	0.28	0.27	0.36	0.28	0.25	0.14	0.27	0.35	0.31	0.33	0.32	0.32	0.33	0.32	**0.42**
					Mother wavelet type: db 10*												
Train	MSE	0.66	0.51	0.54	0.34	0.38	0.39	0.71	0.43	0.40	0.40	0.46	0.36	0.35	0.37	0.35	**0.34**
	RMSE	0.81	0.72	0.73	0.58	0.62	0.62	0.84	0.66	0.63	0.63	0.68	0.60	0.59	0.61	0.60	**0.58**
	MAE	0.64	0.55	0.57	0.45	0.47	0.46	0.66	0.47	0.48	0.48	0.54	0.46	0.45	0.46	0.45	**0.44**
	R^2	0.36	0.50	0.47	0.67	0.63	0.62	0.30	0.58	0.61	0.61	0.55	0.65	0.66	0.37	0.65	**0.67**
Test	MSE	0.61	0.53	0.55	0.33	0.37	0.47	0.85	0.46	0.40	0.46	0.49	0.61	0.36	0.43	0.37	**0.28**
	RMSE	0.78	0.73	0.74	0.58	0.61	0.68	0.92	0.68	0.63	0.67	0.70	0.37	0.60	0.65	0.61	**0.53**
	MAE	0.61	0.58	0.58	0.44	0.48	0.52	0.72	0.52	0.51	0.53	0.54	0.48	0.47	0.51	0.47	**0.43**
	R^2	0.44	0.49	0.46	0.67	0.63	0.55	0.15	0.55	0.60	0.55	0.52	0.63	0.64	0.58	0.63	**0.72**
					Mother wavelet type: Haar												
Train	MSE	0.46	0.41	0.42	0.33	0.35	0.37	0.45	0.37	0.36	0.41	0.41	0.41	0.34	0.37	0.34	**0.37**
	RMSE	0.68	0.64	0.65	0.58	0.59	0.61	0.67	0.61	0.60	0.64	0.64	0.64	0.58	0.61	0.58	**0.61**
	MAE	0.53	0.48	0.49	0.41	0.42	0.44	0.50	0.44	0.43	0.48	0.48	0.48	0.42	0.44	0.42	**0.44**
	R^2	0.55	0.60	0.59	0.67	0.66	0.64	0.56	0.64	0.65	0.59	0.59	0.59	0.67	0.64	0.67	**0.64**
Test	MSE	0.52	0.51	0.53	0.42	0.42	0.43	0.72	0.48	0.44	0.47	0.54	0.42	0.42	0.44	0.42	**0.31**
	RMSE	0.72	0.72	0.73	0.65	0.65	0.66	0.85	0.69	0.66	0.67	0.73	0.65	0.65	0.66	0.65	**0.56**
	MAE	0.56	0.55	0.57	0.50	0.49	0.50	0.65	0.52	0.50	0.52	0.57	0.50	0.50	0.51	0.50	**0.43**
	R^2	0.48	0.49	0.47	0.58	0.58	0.57	0.29	0.53	0.56	0.53	0.47	0.58	0.58	0.56	0.58	**0.69**
					Mother wavelet type: Sym 8												
Train	MSE	0.55	0.47	0.53	0.36	0.37	0.39	0.57	0.41	0.40	0.40	0.46	0.38	0.38	0.40	0.38	**0.38**
	RMSE	0.74	0.69	0.73	0.60	0.61	0.62	0.76	0.64	0.64	0.64	0.68	0.61	0.61	0.63	0.61	**0.61**
	MAE	0.57	0.53	0.57	0.46	0.47	0.48	0.57	0.48	0.49	0.50	0.54	0.47	0.47	0.48	0.47	**0.47**
	R^2	0.46	0.54	0.48	0.65	0.63	0.62	0.44	0.60	0.60	0.61	0.55	0.63	0.63	0.61	0.63	**0.64**
Test	MSE	0.64	0.47	0.53	0.37	0.41	0.44	0.72	0.43	0.43	0.44	0.49	0.39	0.40	0.42	0.39	**0.31**
	RMSE	0.80	0.68	0.73	0.61	0.64	0.66	0.85	0.66	0.65	0.67	0.70	0.62	0.63	0.65	0.62	**0.56**
	MAE	0.59	0.51	0.56	0.48	0.51	0.52	0.66	0.51	0.51	0.51	0.54	0.49	0.50	0.50	0.49	**0.46**
	R^2	0.44	0.54	0.47	0.62	0.59	0.57	0.29	0.57	0.58	0.55	0.51	0.61	0.60	0.58	0.61	**0.68**
					Mother wavelet type: Coif 5												
Train	MSE	0.50	0.45	0.49	0.35	0.36	0.37	0.61	0.38	0.40	0.38	0.42	0.35	0.35	0.36	0.35	**0.36**
	RMSE	0.71	0.67	0.70	0.59	0.60	0.61	0.78	0.62	0.63	0.62	0.65	0.59	0.59	0.60	0.59	**0.60**
	MAE	0.55	0.52	0.55	0.45	0.46	0.47	0.60	0.46	0.49	0.47	0.51	0.45	0.45	0.46	0.45	**0.46**
	R^2	0.51	0.55	0.52	0.66	0.65	0.64	0.40	0.63	0.61	0.63	0.58	0.66	0.66	0.64	0.66	**0.65**
Test	MSE	0.76	0.46	0.57	0.35	0.42	0.49	0.84	0.47	0.43	0.42	0.51	0.42	0.40	0.43	0.41	**0.31**
	RMSE	0.76	0.68	0.75	0.61	0.65	0.7	0.92	0.68	0.66	0.65	0.71	0.64	0.64	0.66	0.64	**0.56**
	MAE	0.59	0.54	0.59	0.48	0.52	0.55	0.73	0.53	0.51	0.50	0.56	0.51	0.50	0.51	0.50	**0.46**
	R^2	0.46	0.55	0.43	0.63	0.58	0.52	0.17	0.53	0.57	0.59	0.56	0.58	0.59	0.56	0.59	**0.67**

* and ** signs indicate the best and worst models, respectively.

Figure 8a,b shows the scatter diagrams of the training and test values of the best stand-alone XGBOOST model at station 1401, respectively. According to the figure, the estimated and actual values deviate significantly from the perfect prediction (the 45^0 lines). This indicates that the stand-alone machine learning model has little predictive power. Figure 8c,d shows the training and test graphics of the wavelet–XGBOOST model obtained using the db10 wavelet and subcomponent inputs. According to these graphs, it is clear that the estimated and actual values overlap better than the stand-alone machine learning model. For this reason, it is interpreted that the wavelet–XGBOOST model can more effectively predict droughts one month later.
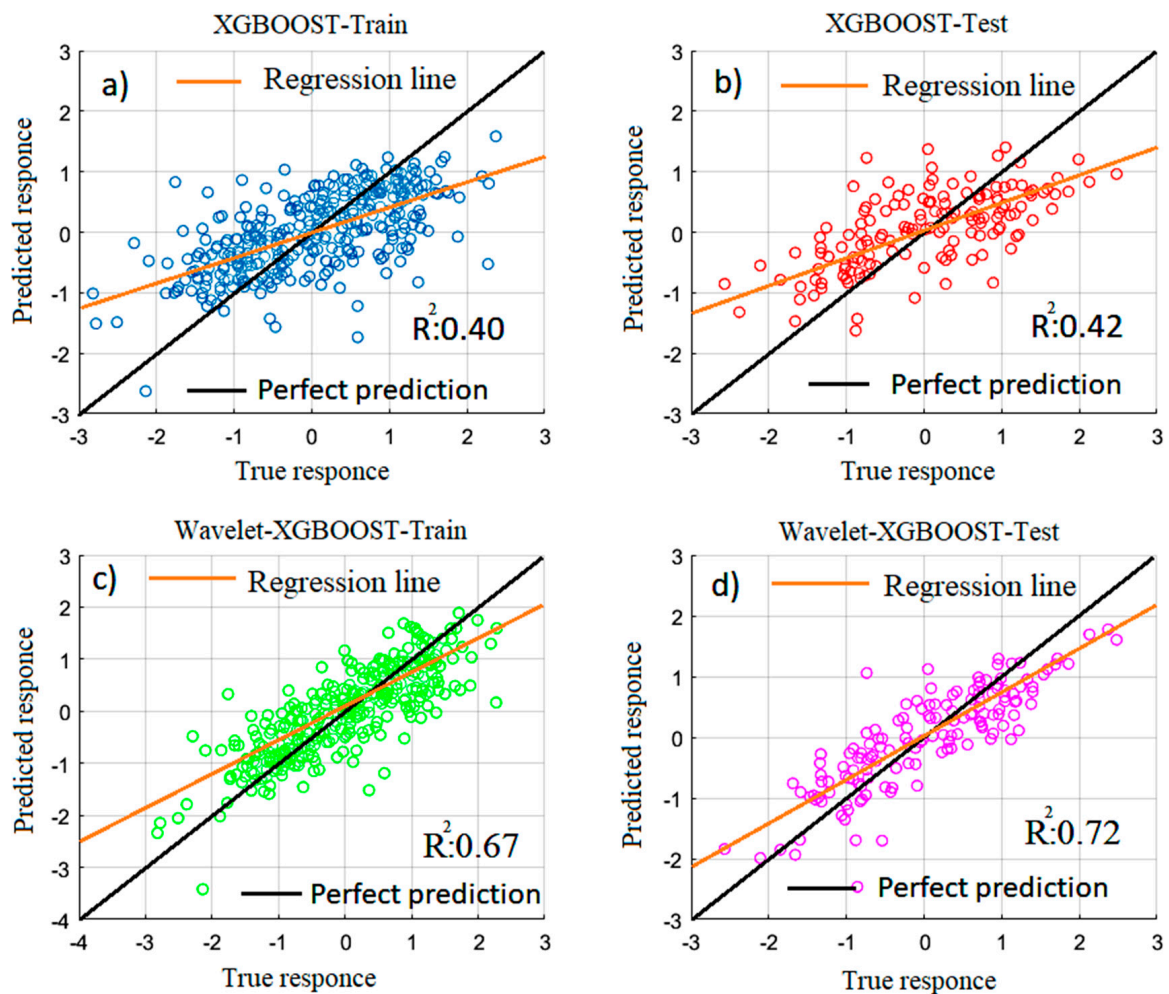
Figure 8. Scatter diagrams of machine learning models for station 1401: (**a**) training the XGBOOST model; (**b**) testing the XGBOOST model, (**c**) tTraining of db 10 wavelet-based LSVR, (**d**) testing of db 10 wavelet-based LSVR.

In Table 7, the drought prediction results at station 1413 are given. According to the performance criteria, the most successful stand-alone model was XGBOOST. In addition, it has been determined that the hybrid wavelet–MGPR model created by using the inputs separated into sub-signals by the db 10 wavelet produces near-perfect prediction results.

The scatter diagrams of the training and test values of the XGBOOST model, which is the best stand-alone machine learning model at station 1413, are shown in Figure 9a,b, respectively. Although the estimated and actual values show a distribution close to the 45^0 lines, deviations have occurred in the values. Figure 9c,d shows training and test graphs of the wavelet–MGPR model obtained using subcomponent inputs with the db10 wavelet. According to these graphs, it is clear that the estimated and actual values overlap. For this reason, it can be said that the wavelet–MGPR model has a near-perfect predictive success of 1-month lead-time droughts.

In Table 8, the drought prediction results at station 1414 are indicated. Statistical criteria such as MSE, RMSE, MAE, and R^2 were tested to select the optimal model. According to these criteria, the optimal stand-alone model was chosen as XGBOOST. Moreover, the XGBOOST model used with the Coif 5 wavelet indicated the best results for predicting SDI values. In addition, the FGSVR model draws attention as the most unsuccessful predicting model.

Table 7. Drought prediction results at the streamflow observation station 1413.

	Method / Statistic	FT	MT	CT	LSVR	QSVR	CSVR	FGSVR**	MGSVR	CGSVR	BT	BAT	SEGPR	MGPR*	EGPR	RQGPR	XGBOOST
								Mother wavelet type: No (Stand-alone ML)								
Train	MSE	0.48	0.42	0.36	0.33	0.33	0.38	0.62	0.36	0.33	0.39	0.37	0.32	0.33	0.46	0.33	**0.33**
	RMSE	0.69	0.65	0.60	0.57	0.58	0.62	0.79	0.60	0.57	0.62	0.61	0.57	0.56	0.59	0.57	**0.56**
	MAE	0.56	0.52	0.47	0.46	0.46	0.47	0.62	0.47	0.45	0.49	0.48	0.45	0.45	0.46	0.45	**0.45**
	R²	0.40	0.48	0.56	0.60	0.59	0.53	0.23	0.55	0.59	0.52	0.54	0.59	0.59	0.57	0.59	**0.68**
Test	MSE	0.68	0.53	0.50	0.40	0.44	0.67	1.47	0.69	0.40	0.49	0.44	0.39	0.39	0.44	0.39	**0.37**
	RMSE	0.82	0.73	0.71	0.63	0.66	0.82	1.21	0.83	0.63	0.70	0.66	0.62	0.63	0.67	0.62	**0.61**
	MAE	0.65	0.58	0.55	0.51	0.53	0.62	0.98	0.65	0.51	0.56	0.53	0.51	0.52	0.54	0.51	**0.48**
	R²	0.31	0.42	0.42	0.51	0.49	0.32	0.05	0.25	0.53	0.45	0.47	0.55	0.54	0.50	0.55	**0.64**
								Mother wavelet type: db 10 *									
Train	MSE	0.04	0.05	0.10	0.007	0.005	0.005	0.13	0.02	0.03	0.03	0.05	0.001	**0.001**	0.009	0.001	0.006
	RMSE	0.19	0.23	0.32	0.09	0.07	0.07	0.36	0.12	0.17	0.18	0.23	0.04	**0.03**	0.09	0.04	0.08
	MAE	0.15	0.18	0.25	0.07	0.06	0.06	0.26	0.10	0.14	0.14	0.18	0.03	**0.03**	0.07	0.03	0.06
	R²	0.95	0.92	0.85	0.99	0.99	0.99	0.80	0.98	0.95	0.95	0.92	0.99	**0.99**	0.99	0.99	0.99
Test	MSE	0.12	0.11	0.22	0.008	0.007	0.03	0.87	0.33	0.06	0.11	0.11	0.007	**0.007**	0.008	0.007	0.005
	RMSE	0.35	0.34	0.47	0.09	0.09	0.17	0.93	0.57	0.24	0.35	0.33	0.08	**0.08**	0.029	0.08	0.07
	MAE	0.26	0.23	0.32	0.07	0.06	0.11	0.65	0.3	0.17	0.19	0.22	0.04	**0.04**	0.18	0.04	0.05
	R²	0.80	0.83	0.67	0.99	0.99	0.97	0.16	0.55	0.96	0.86	0.85	0.99	**0.99**	0.90	0.99	0.99
								Mother wavelet type: Haar									
Train	MSE	0.02	0.05	0.10	0.04	0.04	0.04	0.12	0.04	0.07	0.02	0.10	0.02	0.02	0.01	0.01	**0.18**
	RMSE	0.13	0.23	0.31	0.21	0.21	0.19	0.34	0.20	0.26	0.15	0.32	0.15	0.13	0.12	0.12	**0.42**
	MAE	0.09	0.18	0.25	0.17	0.16	0.14	0.19	0.15	0.21	0.11	0.25	0.05	0.04	0.04	0.04	**0.32**
	R²	0.97	0.91	0.83	0.92	0.92	0.94	0.79	0.93	0.89	0.96	0.83	0.96	0.97	0.98	0.97	**0.83**
Test	MSE	0.41	0.50	0.47	0.34	0.33	0.62	1,44	0.61	0.36	0.46	0.80	0.90	0.66	0.41	0.50	**0.19**
	RMSE	0.64	0.71	0.69	0.58	0.58	0.79	1,20	0.78	0.60	0.68	0.89	0.94	0.81	0.64	0.70	**0.44**
	MAE	0.48	0.52	0.51	0.44	0.44	0.58	0.96	0.59	0.47	0.51	0.72	0.70	0.62	0.50	0.54	**0.33**
	R²	0.49	0.37	0.42	0.58	0.58	0.49	0.001	0.31	0.54	0.42	0.14	0.08	0.24	0.50	0.41	**0.84**
								Mother wavelet type: Sym 8									
Train	MSE	0.27	0.23	0.24	0.16	0.18	0.20	0.30	0.20	0.21	0.21	0.21	0.16	0.16	0.19	0.16	**0.15**
	RMSE	0.52	0.48	0.49	0.40	0.42	0.45	0.55	0.45	0.46	0.45	0.46	0.40	0.40	0.44	0.40	**0.39**
	MAE	0.41	0.38	0.39	0.31	0.32	0.35	0.44	0.35	0.36	0.36	0.36	0.31	0.31	0.34	0.31	**0.31**
	R²	0.67	0.71	0.70	0.79	0.78	0.75	0.62	0.75	0.74	0.74	0.73	0.80	0.80	0.76	0.80	**0.85**
Test	MSE	0.33	0.31	0.41	0.19	0.17	0.33	1.13	0.53	0.26	0.31	0.27	0.18	0.18	0.28	0.18	**0.18**
	RMSE	0.58	0.56	0.64	0.43	0.43	0.58	1.06	0.41	0.51	0.56	0.52	0.43	0.43	0.53	0.43	**0.43**
	MAE	0.45	0.41	0.48	0.33	0.34	0.43	0.82	0.49	0.38	0.40	0.39	0.33	0.33	0.39	0.33	**0.32**
	R²	0.60	0.63	0.50	0.76	0.76	0.58	0.12	0.41	0.73	0.66	0.68	0.77	0.77	0.67	0.77	**0.82**
								Mother wavelet type: Coif 5									
Train	MSE	0.29	0.27	0.26	0.17	0.17	0.19	0.33	0.20	0.22	0.22	0.24	0.17	0.16	0.44	0.17	**0.15**
	RMSE	0.53	0.52	0.51	0.41	0.41	0.44	0.57	0.45	0.46	0.47	0.49	0.41	0.40	0.20	0.41	**0.39**
	MAE	0.42	0.41	0.39	0.32	0.33	0.34	0.46	0.35	0.37	0.37	0.39	0.32	0.31	0.35	0.32	**0.30**
	R²	0.64	0.66	0.67	0.79	0.78	0.76	0.59	0.75	0.73	0.72	0.70	0.79	0.80	0.76	0.79	**0.85**
Test	MSE	0.32	0.3	0.38	0.18	0.18	0.26	1.12	0.53	0.26	0.28	0.27	0.18	0.18	0.28	0.18	**0.19**
	RMSE	0.57	0.54	0.62	0.43	0.43	0.51	1.06	0.73	0.51	0.53	0.52	0.43	0.43	0.53	0.43	**0.44**
	MAE	0.45	0.41	0.46	0.32	0.33	0.38	0.81	0.5	0.38	0.4	0.4	0.32	0.32	0.39	0.32	**0.32**
	R²	0.63	0.65	0.54	0.77	0.77	0.71	0.10	0.4	0.73	0.68	0.69	0.77	0.77	0.68	0.77	**0.82**

* and ** signs indicate the best and worst models, respectively.

When the best models on a station basis were evaluated according to statistical parameters, W–XGBOOST using db 10 mother wavelet at station 1401 (Train: RMSE = 0.58, MAE = 0.44, R² = 0.67, Test: RMSE = 0.53, MAE = 0.43, R² = 0.72), W–MGPR using db 10 mother wavelet at station 1413 (Train: RMSE = 0.03, MAE = 0.03, R² = 0.99, Test: RMSE = 0.08, MAE = 0.04, R² = 0.99), and W–XGBOOST using Coif 5 mother wavelet at station 1414 (Train: RMSE = 0.39, MAE = 0.30, R² = 0.85, Test: RMSE = 0.46, MAE = 0.37, R² = 0.80) were found to be the most successful.

Table 8. Drought prediction results at the streamflow observation station 1414.

	Method / Statistic	FT	MT	CT	LSVR	QSVR	CSVR	FGSVR **	MGSVR	CGSVR	BT	BAT	SEGPR	MGPR	EGPR	RQGPR	XGBOOST *
	Mother wavelet type: No (Stand-alone ML)																
Train	MSE	0.59	0.45	0.41	0.38	0.43	0.44	0.62	0.41	0.38	0.40	0.51	0.38	0.38	0.38	0.39	**0.32**
	RMSE	0.77	0.67	0.64	0.62	0.66	0.66	0.79	0.64	0.62	0.64	0.64	0.61	0.62	0.62	0.63	**0.57**
	MAE	0.61	0.53	0.51	0.48	0.52	0.51	0.64	0.50	0.49	0.51	0.51	0.49	0.49	0.48	0.49	**0.46**
	R^2	0.38	0.53	0.41	0.60	0.54	0.54	0.35	0.56	0.60	0.57	0.57	0.60	0.60	0.60	0.58	**0.68**
Test	MSE	0.54	0.42	0.40	0.32	0.33	0.38	0.92	0.39	0.31	0.35	0.37	0.32	0.32	0.33	0.32	**0.38**
	RMSE	0.73	0.65	0.63	0.57	0.57	0.61	0.96	0.62	0.55	0.60	0.61	0.57	0.56	0.57	0.57	**0.62**
	MAE	0.58	0.51	0.49	0.45	0.45	0.47	0.78	0.48	0.44	0.47	0.48	0.45	0.45	0.45	0.45	**0.47**
	R^2	0.23	0.34	0.34	0.44	0.44	0.36	0.03	0.34	0.45	0.38	0.38	0.44	0.45	0.43	0.44	**0.64**
	Mother wavelet type: db 10																
Train	MSE	0.30	0.28	0.32	0.19	0.20	0.22	0.33	0.22	0.25	0.24	0.29	0.19	0.19	0.22	0.19	**0.16**
	RMSE	0.55	0.53	0.56	0.44	0.45	0.47	0.57	0.47	0.50	0.49	0.53	0.44	0.44	0.47	0.44	**0.40**
	MAE	0.42	0.41	0.43	0.34	0.35	0.35	0.45	0.36	0.39	0.37	0.41	0.34	0.34	0.36	0.34	**0.31**
	R^2	0.68	0.70	0.67	0.80	0.79	0.77	0.65	0.77	0.73	0.74	0.70	0.80	0.80	0.76	0.80	**0.84**
Test	MSE	0.28	0.23	0.24	0.16	0.16	0.17	0.65	0.27	0.18	0.20	0.19	0.15	0.15	0.19	0.15	**0.21**
	RMSE	0.53	0.48	0.49	0.40	0.40	0.41	0.81	0.53	0.43	0.45	0.43	0.39	0.39	0.44	0.39	**0.46**
	MAE	0.40	0.37	0.37	0.30	0.30	0.31	0.60	0.40	0.32	0.33	0.32	0.30	0.30	0.33	0.30	**0.37**
	R^2	0.57	0.61	0.56	0.71	0.71	0.69	0.17	0.55	0.69	0.64	0.66	0.71	0.71	0.67	0.71	**0.79**
	Mother wavelet type: Haar																
Train	MSE	0.33	0.29	0.30	0.25	0.27	0.29	0.34	0.27	0.28	0.30	0.29	0.25	0.25	0.27	0.25	**0.30**
	RMSE	0.57	0.54	0.54	0.50	0.52	0.54	0.58	0.52	0.53	0.55	0.54	0.50	0.50	0.52	0.50	**0.45**
	MAE	0.44	0.41	0.41	0.39	0.39	0.41	0.45	0.39	0.41	0.42	0.42	0.39	0.39	0.40	0.39	**0.35**
	R^2	0.65	0.69	0.69	0.73	0.72	0.69	0.64	0.71	0.70	0.68	0.69	0.73	0.73	0.71	0.73	**0.80**
Test	MSE	0.22	0.29	0.25	0.17	0.18	0.19	0.77	0.33	0.22	0.21	0.22	0.17	0.17	0.23	0.17	**0.25**
	RMSE	0.47	0.54	0.50	0.41	0.43	0.44	0.88	0.57	0.47	0.46	0.47	0.41	0.41	0.48	0.41	**0.50**
	MAE	0.34	0.39	0.38	0.31	0.32	0.33	0.68	0.42	0.65	0.33	0.35	0.31	0.31	0.35	0.31	**0.37**
	R^2	0.60	0.48	0.53	0.68	0.67	0.65	0.10	0.42	0.63	0.61	0.59	0.69	0.69	0.61	0.69	**0.75**
	Mother wavelet type: Sym 8																
Train	MSE	0.30	0.29	0.28	0.19	0.20	0.22	0.35	0.22	0.24	0.23	0.26	0.19	0.19	0.22	0.19	**0.15**
	RMSE	0.55	0.53	0.52	0.43	0.45	0.46	0.59	0.47	0.49	0.48	0.51	0.43	0.43	0.47	0.43	**0.39**
	MAE	0.43	0.42	0.41	0.34	0.35	0.35	0.46	0.36	0.38	0.38	0.40	0.34	0.34	0.37	0.34	**0.30**
	R^2	0.68	0.70	0.71	0.80	0.79	0.77	0.63	0.77	0.75	0.75	0.72	0.80	0.80	0.76	0.80	**0.85**
Test	MSE	0.34	0.21	0.27	0.15	0.15	0.16	0.66	0.27	0.19	0.18	0.19	0.15	0.15	0.19	0.15	**0.21**
	RMSE	0.58	0.46	0.52	0.39	0.39	0.41	0.81	0.52	0.43	0.42	0.44	0.39	0.39	0.44	0.39	**0.46**
	MAE	0.46	0.35	0.39	0.29	0.3	0.30	0.6	0.39	0.33	0.3	0.61	0.29	0.29	0.33	0.29	**0.37**
	R^2	0.47	0.61	0.51	0.71	0.72	0.70	0.16	0.56	0.69	0.67	0.65	0.72	0.72	0.68	0.72	**0.79**
	Mother wavelet type: Coif 5*																
Train	MSE	0.30	0.24	0.28	0.19	0.20	0.20	0.31	0.21	0.24	0.23	0.27	0.19	0.19	0.22	0.19	**0.15**
	RMSE	0.54	0.49	0.53	0.43	0.44	0.45	0.56	0.46	0.49	0.48	0.52	0.43	0.43	0.46	0.43	**0.39**
	MAE	0.43	0.39	0.42	0.34	0.35	0.34	0.45	0.36	0.38	0.37	0.40	0.34	0.34	0.36	0.34	**0.30**
	R^2	0.69	0.75	0.70	0.80	0.79	0.79	0.67	0.78	0.75	0.76	0.72	0.80	0.80	0.77	0.80	**0.85**
Test	MSE	0.35	0.24	0.26	0.15	0.15	0.15	0.65	0.26	0.19	0.19	0.20	0.15	0.15	0.19	0.15	**0.21**
	RMSE	0.59	0.49	0.51	0.39	0.39	0.39	0.81	0.51	0.43	0.44	0.45	0.39	0.39	0.43	0.39	**0.46**
	MAE	0.46	0.36	0.38	0.29	0.30	0.28	0.60	0.38	0.33	0.32	0.33	0.29	0.29	0.33	0.29	**0.37**
	R^2	0.47	0.57	0.54	0.72	0.72	0.73	0.16	0.57	0.70	0.65	0.63	0.72	0.72	0.68	0.72	**0.80**

* and ** signs indicate the best and worst models, respectively.

In Figure 10a,b, scatter diagrams are presented for the XGBOOST model, the best stand-alone machine learning model at station 1414. It is seen in Figure 10 that the estimated and actual values deviate significantly from the perfect prediction line. This indicates that the prediction success of the stand-alone machine learning model is low. Figure 10c,d shows the training and test graphics of the wavelet–XGBOOST model, which is obtained using the inputs separated into subcomponents by the Coif-5 wavelet. According to these graphs, it is seen that the estimated and actual values represent the perfect prediction line better than the stand-alone machine learning model. This indicates that the discrete wavelet transform increases the prediction performance of 1-month lead-time droughts.
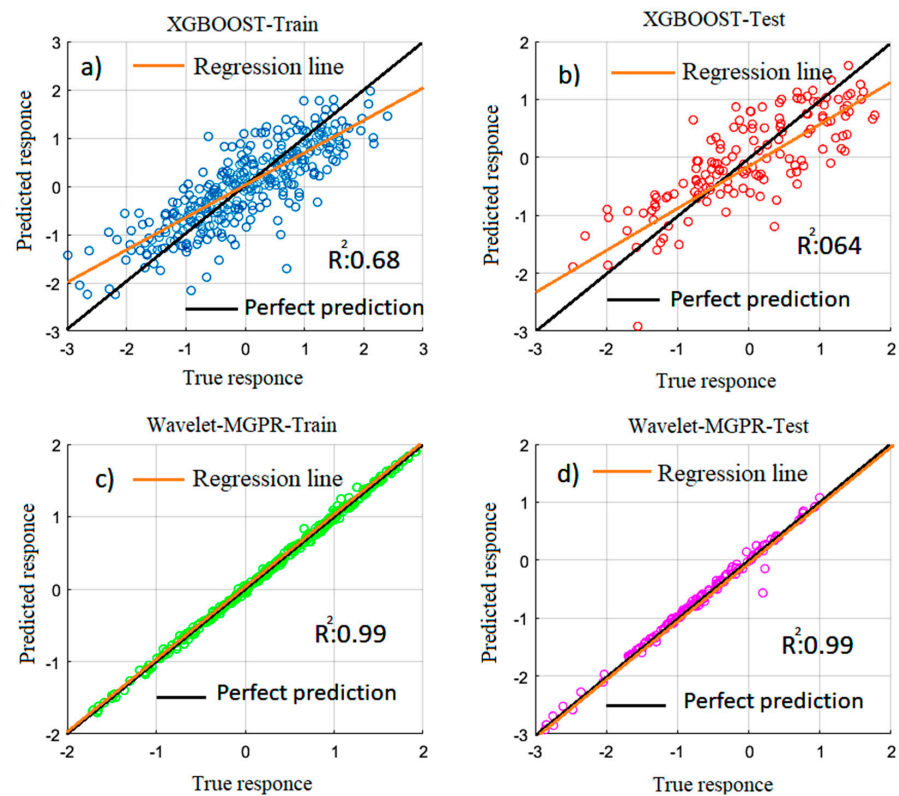
Figure 9. Scatter diagrams of machine learning models for station 1413: (**a**) training the SEGPR model; (**b**) testing the SEGPR model; (**c**) training of db 10 wavelet-based MGPR; (**d**) testing of db 10 wavelet-based MGPR.
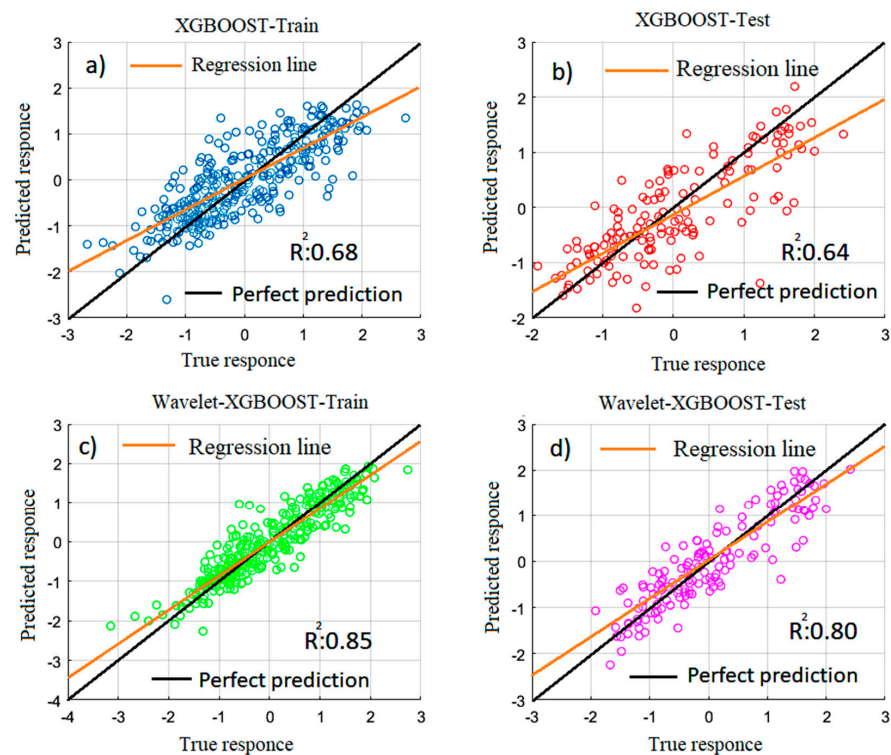

Figure 10. Scatter diagrams of machine learning models for station 1414: (**a**) training the XGBOOST model; (**b**) testing the XGBOOST model; (**c**) training of wavelet-based XGBOOST; (**d**) testing of wavelet-based XGBOOST.

5. Discussion

In this study, various machine learning models and the combination of these models with wavelet transform are compared to predict hydrological droughts with 1-month lead-time. When the literature is examined, it is clear that hybrid wavelet–artificial intelligence techniques, which are established using inputs decomposed by wavelet transform, are superior to single AIs in drought prediction. [17,22,28,68]. In this respect, the study results are in line with the literature.

When the performances of the mother wavelets used in drought predicting are evaluated, Djerbouai and Souag-Gamane [22] applied Haar (db1) and Daubechies (db-n, n values between 2 and 17) mother wavelets to predict SPI values of 3, 6, and 12 months at different lead-times. db15 and db13 mother wavelets showed the most successful results in SPI prediction. Ahmadi and Mehdizadeh [28] employed wavelet-based hybrid models to predict RDI values in Iran. For this purpose, the RDI series are predicted by Haar, Daubechies (db2, db4), Coifflet, Symlet, and Fejer–Korovkin wavelets. As a result, while Coifflet and db4 wavelets performed the best, F-K and Haar wavelets performed the worst. Studies of Djerbouai and Souag-Gamane [22] and Ahmadi and Mehdizadeh [29] support the study in terms of showing the superiority of the Daubechies wavelet in drought prediction.

When various machine learning models are evaluated in drought prediction, Borji, Malekian [16] applied ANN and SVM to predict long-term droughts in Iran's Latian watershed. It has been determined that the SVM model is successful in predicting drought; the SVM model (RMSE: 0.40) showed more accurate prediction results than ANN (RMSE: 0.42) in estimating short-term SDI. While the obtained findings overlap with stations 1401 and 1414, they contradict station 1413 of the current study. The contradiction encountered can be explained by the difference in the time scale used in the SDI values. Hezarani et al. [69] applied the ANN method to predict the standardized precipitation index (SPI)-based meteorological and hydrological drought in the Yesilirmak River basin of Turkey. While the FFNN model successfully predicts meteorological drought calculated with SPI, it is ineffective in predicting hydrological drought. As the study of Hezarani et al. [69] used SPI values to predict hydrological droughts, the prediction performance was poor compared to the current research. This shows that SDI values are more effective than SPI in predicting hydrological drought. Belayneh et al. [70] used wavelet transform ANN and SVM models to predict droughts in Ethiopia's Awash River basin. It has been determined that the wavelet-boosting ANN and wavelet-boosting SVR models outperform other models in predicting droughts. Aghelpour, Bahrami-Pichaghchi, Varshavian, and Assessment [5] compared ANFIS and GMDH to predict SDI-based hydrological droughts in the Khalkaei and Pasikha rivers and found the estimated results of the two models to be highly similar; the best GMDH model attained RMSE: 0.512 and ANFIS, RMSE: 0.543, in monthly SDI prediction. Aghelpour, Bahrami-Pichaghchi, and Varshavian [5] determined that the stand alone SVM, GPR, BT, BAT, and XGBOOST and hybrid wavelet–SVM, GPR, BT, BAT, and XGBOOST models outperformed the GMDH and ANFIS models. The XGBOOST algorithm showed the most successful results, even though the stations used had different flow status and models were built using different delayed streamflow values. In addition, the wavelet-based XGBOOST hybrid model showed superior results in all stations.

6. Conclusions

This study applied various machine learning and hybrid wavelet–machine learning techniques to predict SDI-based hydrological droughts in the Yesilirmak basin. The input variables are divided into subcomponents with Haar, Db10, Sym8, and Coif5 mother wavelets and presented as inputs to the models to develop the hybrid wavelet-based machine learning model. The results of the study are expressed as follows:

- This study proves that the wavelet-based machine learning model successfully predicts drought;

- According to the ACF and PACF graphs, it has been deduced that SDI values with a lag of 1, 2, 3, 4, 8, 9, 10, 11, and 12 months can be used effectively in drought-predicting models;
- The wavelet-based machine learning model has proven to be successful in drought predicting;
- It has been determined that the drought prediction success of machine learning models increases when inputs separated into sub-signals by the discrete wavelet transform are used;
- The best stand-alone machine learning techniques were obtained by comparing various statistical parameters as XGBOOST;
- Hybrid wavelet–MGPR and XGBOOST models were the best models to predict the SDI value during the 1-month lead-time in the Yesilirmak basin;
- When the performances of different mother wavelets (db10, Haar, Sym8, and Coif5) were compared, it was revealed that the db10 wavelet was the best in drought prediction;
- All selected model combinations gave realistic results in the prediction of droughts. In addition, the highest prediction accuracy (R^2:0.99) was obtained with the combination of f (SDI(t-10), SDI(t-8), SDI(t-3), SDI(t-2), SDI(t-1), and SDI(t))= SDI(t + 1) *in* 1413 no streamflow observation station;
- The FGSVR model was notably the worst prediction model. In addition, the wavelet–FGSVR model does not have sufficient prediction accuracy.

The study's outputs constitute an essential resource for water managers and policymakers to manage drought and water resources, take precautions against droughts, combat climate change, increase agricultural production efficiency, and assess the risk of forest fires in the Yeşilırmak basin, which has a mountainous structure.

For future studies: (i) different mother wavelets can be used in drought prediction; (ii) drought prediction success can be evaluated with different drought indices and long-term lead-time; (iii) the success of bio-inspired algorithms in drought prediction can be compared.

Abbreviations

DrinC	Drought indices calculator
ANNs	Artificial neural networks
PHDI	Palmer hydrological drought index
SWSI	Surface water supply index
SRI	Standardized runoff index
SDI	Streamflow drought index
CANFIS	Coactive neuro-fuzzy inference system
MLPNN	Multi-layer perceptron neural network
MLR	Multiple linear regression
WD	Wavelet decomposition

SVM	Support vector machine
EMD	Empirical mode decomposition
ANFIS	Adaptive neuro-fuzzy inference system
GMDH	Group method of data handling
XGBOOST	eXtreme gradient boosting
GPR	Gaussian processes regression
RT	Regression tree
ET	Ensembles of trees
MSE	Mean square error
RMSE	Root means square error
MAE	Mean absolute error
ACF	Autocorrelation functions
PACF	Partial autocorrelation functions

References

1. Bryant, E. *Natural Hazards*, 2nd ed.; Cambridge University Press: Cambridge, UK, 2004. [CrossRef]
2. Morid, S.; Smakhtin, V.; Bagherzadeh, K. Drought forecasting using artificial neural networks and time series of drought indices. *Int. J. Climatol. A J. R. Meteorol. Soc.* **2007**, *27*, 2103–2111. [CrossRef]
3. Karavitis, C.A.; Alexandris, S.; Tsesmelis, D.E.; Athanasopoulos, G. Application of the standardized precipitation index (SPI) in Greece. *Water* **2011**, *3*, 787–805.
4. Khan, M.M.H.; Muhammad, N.S.; El-Shafie, A. Wavelet based hybrid ANN-ARIMA models for meteorological drought forecasting. *J. Hydrol.* **2020**, *590*, 125380. [CrossRef]
5. Aghelpour, P.; Bahrami-Pichaghchi, H.; Varshavian, V. Hydrological drought forecasting using multi-scalar streamflow drought index, stochastic models and machine learning approaches, in northern Iran. *Stoch. Environ. Res. Risk Assess.* **2021**, 1–21. [CrossRef]
6. Yevjevich, V.M. *Objective Approach to Definitions and Investigations of Continental Hydrologic Droughts*; Hydrology Paper 1967, no. 23; Colorado State University: Fort Collins, CO, USA, 1967.
7. Tallaksen, L.M.; Van Lanen, H.A. *Hydrological Drought: Processes and Estimation Methods for Streamflow and Groundwater*; Developments in Water Sciences 48; Elsevier Science B.V.: Amsterdam, The Netherlands, 2004; 580p.
8. Fleig, A. *Hydrological Drought–A Comparative Study Using Daily Discharge Series from around the World*; Der Albert-Ludwigs-Universität Freiburg i. Br: Breisgau, Germany, 2004.
9. Nalbantis, I. Evaluation of a hydrological drought index. *Eur. Water* **2008**, *23*, 67–77.
10. Shamshirband, S.; Hashemi, S.; Salimi, H.; Samadianfard, S.; Asadi, E.; Shadkani, S.; Kargar, K.; Mosavi, A.; Nabipour, N.; Chau, K.-W. Predicting standardized streamflow index for hydrological drought using machine learning models. *Eng. Appl. Comput. Fluid Mech.* **2020**, *14*, 339–350. [CrossRef]
11. Nalbantis, I.; Tsakiris, G. Assessment of hydrological drought revisited. *Water Resour. Manag.* **2009**, *23*, 881–897. [CrossRef]
12. Myronidis, D.; Ioannou, K.; Fotakis, D.; Dörflinger, G. Streamflow and hydrological drought trend analysis and forecasting in Cyprus. *Water Resour. Manag.* **2018**, *32*, 1759–1776. [CrossRef]
13. Tabari, H.; Nikbakht, J.; Hosseinzadeh Talaee, P. Hydrological drought assessment in Northwestern Iran based on streamflow drought index (SDI). *Water Resour. Manag.* **2013**, *27*, 137–151.
14. Jahangir, M.H.; Yarahmadi, Y. Hydrological drought analyzing and monitoring by using Streamflow Drought Index (SDI) (case study: Lorestan, Iran). *Arab. J. Geosci.* **2020**, *13*, 1–12. [CrossRef]
15. Mishra, A.K.; Singh, V.P. A review of drought concepts. *J. Hydrol.* **2010**, *391*, 202–216. [CrossRef]
16. Borji, M.; Malekian, A.; Salajegheh, A.; Ghadimi, M. Multi-time-scale analysis of hydrological drought forecasting using support vector regression (SVR) and artificial neural networks (ANN). *Arab. J. Geosci.* **2016**, *9*, 1–10. [CrossRef]
17. Belayneh, A.; Adamowski, J.; Khalil, B.; Ozga-Zielinski, B. Long-term SPI drought forecasting in the Awash River Basin in Ethiopia using wavelet neural network and wavelet support vector regression models. *J. Hydrol.* **2014**, *508*, 418–429. [CrossRef]
18. Mishra, A.; Desai, V.; Singh, V.J. Drought forecasting using a hybrid stochastic and neural network model. *J. Hydrol. Eng.* **2007**, *12*, 626–638. [CrossRef]
19. Fung, K.F.; Huang, Y.F.; Koo, C.H. Coupling fuzzy–SVR and boosting–SVR models with wavelet decomposition for meteorological drought prediction. *Environ. Earth Sci.* **2019**, *78*, 1–18. [CrossRef]
20. Mohamadi, S.; Sammen, S.S.; Panahi, F.; Ehteram, M.; Kisi, O.; Mosavi, A.; Ahmed, A.N.; El-Shafie, A.; Al-Ansari, N.J.N.H. Zoning map for drought prediction using integrated machine learning models with a nomadic people optimization algorithm. *Nat. Hazards* **2020**, *104*, 537–579. [CrossRef]
21. Dehghani, M.; Saghafian, B.; Rivaz, F.; Khodadadi, A. Evaluation of dynamic regression and artificial neural networks models for real-time hydrological drought forecasting. *Arab. J. Geosci.* **2017**, *10*, 1–13. [CrossRef]
22. Djerbouai, S.; Souag-Gamane, D. Drought forecasting using neural networks, wavelet neural networks, and stochastic models: Case of the Algerois Basin in North Algeria. *Water Resour. Manag.* **2016**, *30*, 2445–2464. [CrossRef]

23. Hong, X.; Guo, S.; Zhou, Y.; Xiong, L. Uncertainties in assessing hydrological drought using streamflow drought index for the upper Yangtze River basin. *Stoch. Environ. Res. Risk Assess.* **2015**, *29*, 1235–1247. [CrossRef]

24. Malik, A.; Kumar, A.; Singh, R.P. Application of heuristic approaches for prediction of hydrological drought using multi-scalar streamflow drought index. *Water Resour. Manag.* **2019**, *33*, 3985–4006. [CrossRef]

25. Wirsing, K. Time frequency analysis of wavelet and Fourier transform. In *Wavelet Theory*; IntechOpen: London, UK, 2020.

26. Özger, M.; Başakın, E.E.; Ekmekcioğlu, Ö.; Hacısüleyman, V. Comparison of wavelet and empirical mode decomposition hybrid models in drought prediction. *Comput. Electron. Agric.* **2020**, *179*, 105851. [CrossRef]

27. Malik, A.; Kumar, A. Meteorological drought prediction using heuristic approaches based on effective drought index: A case study in Uttarakhand. *Arab. J. Geosci.* **2020**, *13*, 1–17. [CrossRef]

28. Ahmadi, F.; Mehdizadeh, S.; Mohammadi, B. Development of Bio-Inspired-and Wavelet-Based Hybrid Models for Reconnaissance Drought Index Modeling. *Water Resour. Manag.* **2021**, *35*, 4127–4147. [CrossRef]

29. Karbasi, M.; Karbasi, M.; Jamei, M.; Malik, A.; Azamathulla, H.M. Development of a new wavelet-based hybrid model to forecast multi-scalar SPEI drought index (case study: Zanjan city, Iran). *Theor. Appl. Clim.* **2021**, *147*, 499–522. [CrossRef]

30. Achite, M.; Banadkooki, F.B.; Ehteram, M.; Bouharira, A.; Ahmed, A.N.; Elshafie, A. Exploring Bayesian model averaging with multiple ANNs for meteorological drought forecasts. *Stoch. Environ. Res. Risk Assess.* **2022**, *36*, 1835–1860. [CrossRef]

31. Elbeltagi, A.; Kumar, M.; Kushwaha, N.L.; Pande, C.B.; Ditthakit, P.; Vishwakarma, D.K.; Subeesh, A. Drought indicator analysis and forecasting using data driven models: Case study in Jaisalmer, India. *Stoch. Environ. Res. Risk Assess.* **2022**, 1–19. [CrossRef]

32. Kumar, R.; Kumar, A.; Shankhwar, A.K.; Vishkarma, D.K.; Sachan, A.; Singh, P.; Jahangeer, J.; Verma, A.; Kumar, V. Modelling of meteorological drought in the foothills of Central Himalayas: A case study in Uttarakhand State, India. *Ain Shams Eng. J.* **2022**, *13*, 101595. [CrossRef]

33. Katipoğlu, O.M. Monthly streamfow prediction in Amasya, Türkiye, using an integrated approach of a feedforward backpropagation neural network and discrete wavelet transform. *Model. Earth Syst. Environ.* **2022**. [CrossRef]

34. Serencam, U. Innovative trend analysis of total annual rainfall and temperature variability case study: Yesilirmak region, Turkey. *Arabian J. Geosci.* **2019**, *12*, 1–9. [CrossRef]

35. Üstündağ, S. Comparative trend analysis of temperature, precipitation, evaporation and flow data in Yeşilırmak Basin. Master's Thesis, Karabuk University Graduate, School of Education Department of Geography, Karabuk, Turkey, 2022.

36. Boustani, A.; Ulke, A. Investigation of meteorological drought indices for environmental assessment of Yesilirmak Region. *J. Environ. Treat. Tech.* **2020**, *8*, 374–381.

37. Katipoglu, O.M.; Yeşilyurt, S.N.; Dalkılıç, H.Y. Trend analysis of hydrological droughts in Yeşilırmak basin by Mann Kendall and Sen Innovative Trend Analysis. *Gumushane Univ. J. Sci.* **2022**, *12*, 422–442.

38. McKee, T.B.; Doesken, N.J.; Kleist, J. The relationship of drought frequency and duration to time scales. In Proceedings of the 8th Conference on Applied Climatology, Anaheim, CA, USA, 17–22 January 1993; pp. 179–183.

39. Gaona, J.; Quintana-Segui, P.; Escorihuela, J.M.; Boone, A.; Llasat, M.C. Interactions between precipitation, evapotranspiration and soil moisture-based indices to characterize drought with high-resolution remote sensing and land-surface model data. *Nat. Hazards Earth Syst. Sci. Discuss.* **2022**, *22*, 3461–3485. [CrossRef]

40. Zucco, G.; Brocca, L.; Moramarco, T.; Morbidelli, R. Influence of land use on soil moisture spatial–temporal variability and monitoring. *J. Hydrol.* **2014**, *516*, 193–199. [CrossRef]

41. Landeras, G.; Ortiz-Barredo, A.; López, J.J. Forecasting weekly evapotranspiration with ARIMA and artificial neural network models. *J. Irrig. Drain. Eng.* **2009**, *135*, 323–334. [CrossRef]

42. Deo, R.C.; Tiwari, M.K.; Adamowski, J.F.; Quilty, J.M. Forecasting effective drought index using a wavelet extreme learning machine (W-ELM) model. *Stoch. Environ. Res. Risk Assess.* **2017**, *31*, 1211–1240. [CrossRef]

43. Vapnik, V. *The Nature of Statistical Learning Theory*; Springer: Cham, Switzerland, 2013.

44. Wang, L. *Support Vector Machines: Theory and Applications*; Springer: Cham, Switzerland, 2005; Volume 177.

45. Muller, K.-R.; Mika, S.; Ratsch, G.; Tsuda, K.; Scholkopf, B. An introduction to kernel-based learning algorithms. *IEEE Trans. Neural Networks* **2001**, *12*, 181–201. [CrossRef]

46. MathWorks. Statistics and Machine Learning Toolbox™ User's Guide. Available online: https://www.mathworks.com/help/pdf_doc/stats/stats.pdf (accessed on 17 November 2022).

47. Kushwaha, N.L.; Rajput, J.; Elbeltagi, A.; Elnaggar, A.Y.; Sena, D.R.; Vishwakarma, D.K.; Mani, I.; Hussein, E.E. Data intelligence model and meta-heuristic algorithms-based pan evaporation modelling in two different agro-climatic zones: A case study from Northern India. *Atmosphere* **2021**, *12*, 1654. [CrossRef]

48. Fairbrother, J.; Nemeth, C.; Rischard, M.; Brea, J.; Pinder, T. GaussianProcesses. jl: A Non-parametric Bayes package for the Julia Language. *J. Stat. Softw.* **2022**, *102*, 1–36. [CrossRef]

49. Chen, J.; Li, M.; Wang, W. Statistical uncertainty estimation using random forests and its application to drought forecast. *Math. Probl. Eng.* **2012**, *2012*, 915053. [CrossRef]

50. Zhang, N.; Leatham, K. Neurodynamics-Based Nonnegative Matrix Factorization for Classification. In *International Conference on Neural Information Processing*; Springer: Cham, Switzerland, 2018; pp. 519–529.

51. Rasmussen, C.E.; Williams, C. *Gaussian Processes for Machine Learning*; MIT Press: Cambridge, MA, USA, 2006; Volume 1.

52. Gao, W.; Karbasi, M.; Hasanipanah, M.; Zhang, X.; Guo, J. Developing GPR model for forecasting the rock fragmentation in surface mines. *Eng. Comput.* **2018**, *34*, 339–345. [CrossRef]

53. Subbarao, M.V.; Samundiswary, P. Automatic modulation recognition in cognitive radio receivers using multi-order cumulants and decision trees. *Int. J. Rec. Technol. Eng. (IJRTE)* **2018**, *7*, 61–69.

54. Zounemat-Kermani, M.; Batelaan, O.; Fadaee, M.; Hinkelmann, R. Ensemble machine learning paradigms in hydrology: A review. *J. Hydrol.* **2021**, *598*, 126266. [CrossRef]

55. Naghibi, S.A.; Pourghasemi, H.R.; Dixon, B. GIS-based groundwater potential mapping using boosted regression tree, classification and regression tree, and random forest machine learning models in Iran. *Environ. Monit. Assess.* **2016**, *188*, 1–27. [CrossRef] [PubMed]

56. Alnahit, A.O.; Mishra, A.K.; Khan, A.A. Stream water quality prediction using boosted regression tree and random forest models. *Stoch. Environ. Res. Risk Assess.* **2022**, *36*, 2661–2680. [CrossRef]

57. Elbeltagi, A.; Kumari, N.; Dharpure, J.K.; Mokhtar, A.; Alsafadi, K.; Kumar, M.; Mehdinejadiani, B.; Ramezani Etedali, H.; Brouziyne, Y.; Towfiqul Islam, A.R.M. Prediction of combined terrestrial evapotranspiration index (CTEI) over large river basin based on machine learning approaches. *Water* **2021**, *13*, 547. [CrossRef]

58. Carrera, B.; Kim, K. Comparison analysis of machine learning techniques for photovoltaic prediction using weather sensor data. *Sensors* **2020**, *20*, 3129. [CrossRef]

59. Qian, N.; Wang, X.; Fu, Y.; Zhao, Z.; Xu, J.; Chen, J. Predicting heat transfer of oscillating heat pipes for machining processes based on extreme gradient boosting algorithm. *Appl. Therm. Eng.* **2020**, *164*, 114521. [CrossRef]

60. Essam, Y.; Ahmed, A.N.; Ramli, R.; Chau, K.-W.; Idris Ibrahim, M.S.; Sherif, M.; Sefelnasr, A.; El-Shafie, A. Investigating photovoltaic solar power output forecasting using machine learning algorithms. *Eng. Appl. Comput. Fluid Mech.* **2022**, *16*, 2002–2034. [CrossRef]

61. Sang, Y.-F. A review on the applications of wavelet transform in hydrology time series analysis. *Atmos. Res.* **2013**, *122*, 8–15. [CrossRef]

62. Das, P.; Naganna, S.R.; Deka, P.C.; Pushparaj, J. Hybrid wavelet packet machine learning approaches for drought modeling. *Environ. Earth Sci.* **2020**, *79*, 1–18. [CrossRef]

63. Tiwari, M.K.; Chatterjee, C. Development of an accurate and reliable hourly flood forecasting model using wavelet–bootstrap–ANN (WBANN) hybrid approach. *J. Hydrol.* **2010**, *394*, 458–470. [CrossRef]

64. Nourani, V.; Alami, M.T.; Aminfar, M.H. A combined neural-wavelet model for prediction of Ligvanchai watershed precipitation. *Eng. Appl. Artif. Intell.* **2009**, *22*, 466–472. [CrossRef]

65. Elbeltagi, A.; Kushwaha, N.L.; Rajput, J.; Vishwakarma, D.K.; Kulimushi, L.C.; Kumar, M.; Zhang, J.; Pande, C.B.; Choudhari, P.; Meshram, S.G.; et al. Modelling daily reference evapotranspiration based on stacking hybridization of ANN with meta-heuristic algorithms under diverse agro-climatic conditions. *Stoch. Environ. Res. Risk Assess.* **2022**, *36*, 3311–3334. [CrossRef]

66. Singh, A.K.; Kumar, P.; Ali, R.; Al-Ansari, N.; Vishwakarma, D.K.; Kushwaha, K.S.; Panda, K.C.; Sagar, A.; Mirzania, E.; Elbeltagi, A.; et al. An Integrated Statistical-Machine Learning Approach for Runoff Prediction. *Sustainability* **2022**, *14*, 8209. [CrossRef]

67. Partal, T.; Kişi, Ö. Wavelet and neuro-fuzzy conjunction model for precipitation forecasting. *J. Hydrol.* **2007**, *342*, 199–212. [CrossRef]

68. Belayneh, A.; Adamowski, J. Standard precipitation index drought forecasting using neural networks, wavelet neural networks, and support vector regression. *Appl. Comput. Intell. Soft Comput.* **2012**, *2012*, 794061. [CrossRef]

69. Hezarani, A.B.; Zeybekoğlu, U.; Keskin, A.Ü. Hydrological and Meteorological Drought Forecasting for the Yesilirmak River Basin, Turkey. *J. Sustain. Eng. Pract. Technol. Dev.* **2021**, *4*, 121–135.

70. Belayneh, A.; Adamowski, J.; Khalil, B.; Quilty, J. Coupling machine learning methods with wavelet transforms and the bootstrap and boosting ensemble approaches for drought prediction. *Atmos. Res.* **2016**, *172*, 37–47. [CrossRef]